Defining Good Neighbours: Modelling Root Traits for Beneficial Plant-Plant Interactions

Karolína Benková, Liz Howell, Andrés Miniguano Trujillo*

Supervised by Dr Mariya Ptashnyk†

In collaboration with Dr Tim George‡ and Dr Alison Karley‡

*Maxwell Institute for Mathematical Sciences, {K.Benkova,Liz.Howell,Andres.Miniguano-Trujillo}@ed.ac.uk
†Heriot-Watt University, M.Ptashnyk@hw.ac.uk
‡The James Hutton Institute, {Tim.George,Ali.Karley}@hutton.ac.uk

Executive summary

The issue of nutrient deficiency is one that plagues the modern world, and it will only increase in importance as the world expands and people begin to grow crops in increasingly harsh climates. Improving the way that plants make use of the nutrients in the soil may allow them to flourish even in soils of lesser quality. In addition, if plants can gather additional nutrients, they can pass them on to those that consume them, as it happens with zinc. Thus, finding ways to improve the efficiency of roots absorbing nutrients could be of huge benefit as the need for dietary supplements or fertilisers would decrease.

This report presents research considering two mathematical models of nonlinear partial differential equations which describe interaction of one or two root exudates with a micronutrient that is absorbed by the root. We study two intercropping combinations, first rice-rice, and then barley-tobacco crops. This work thus reports on biological background of the plants and chemicals concerned, the corresponding mathematical models for intercropping, their computational results obtained by solving the systems numerically, and on the existence and non-negativity of solutions. The results we describe can be used as a guidance for choosing suitable plant combinations and soils for beneficial intercropping with enhanced nutrient uptake, giving leads for further study of the problem in future work.

The main objective of the numerical experiments is to find the relationship between the parameters and the nutrient absorbed by the root. Thus, we create plots for cumulative uptake of nutrients by the root, and additionally we examine concentrations of the chemicals in between the two roots. The simulations are done using the computing platform FEniCS with its Python interface, while the visualisations are done using Paraview and Python's Matplotlib library.

First, we modify an existing model by adding another identical root, and examine the effects of changing the proximity of the roots and the exudation rate. We use parameters modelling zinc uptake from zinc-deficient soils by rice plants, using the phytosiderophore DMA. We find that positive effects of intercropping are largely lost once plants are too far from each other, i.e. when their zones of root influence don't intersect anymore. However, if the expression of genes related to DMA expression is increased, this may lead to a small increase in the maximum distance between plants where intercropping is effective. Increasing the expression of genes relating to zinc uptake rate however is not as effective at making a difference in cumulative zinc absorption, as nutrient uptake depends on how much nutrients are available in the soil, which depends primarily on the exudation rate.

Next, we derive a model for two exudates as this is both more interesting and complex scenario dynamics-wise. We choose the parameters to model roots of tobacco and barley and carry numerical simulations changing a wide range of parameters to model interactions of the exudates citrate and phytase with the nutrient phosphate. In addition to the results in the previous paragraph we find that that for higher nutrient uptake, increased exudation rate of the roots and increased diffusion and buffer power of the nutrient are important, along with decreased buffer power and diffusion of the exudates. We acknowledge the limitations of the model and the results being an approximation of the real dynamics in the rhizosphere because of the number of assumptions we have made.

Finally, the existence of solutions for the nonlinear systems is studied at the end of the document. Using a general framework, it is proved that all the coupled differential systems studied in this work have a unique solution. Additional analyses were carried out, showing that solutions are bounded and non-negative for bounded non-negative initial data.

Abstract

The issue of nutrient deficiency in plants and an effective uptake of nutrients from the soil is a problem affecting crop-focused industries in the modern age. This project is concerned with expanding an existing model for nutrient extraction using one exudate-producing root into a two root system. First, a set of boundary conditions is added to model another root and experiment with the proximity of two identical roots and the exudation rate with the intention to model intercropping. Then we derive a system with two exudates produced by two roots which we use for further numerical experiments with the model's parameters. Overall, we find that planting at a close enough distance that the zones of root influence interact is key to encouraging a mutually beneficial relationship between roots. The results also show that for higher nutrient uptake, increased exudation rate of the roots and increased diffusion and buffer power of the nutrient are important, along with decreased buffer power and diffusion of the exudates. Finally, an analysis of the system provides us with a proof of existence of a solution.

Contents

1 Introduction

Nutrient deficiency is one of the most pressing problems affecting crops in the modern age. In particular, humans rely upon grasses and grains to introduce zinc (Zn) and other key nutrients to our diets. Thus, as our population grows, we would like to plant more crops to feed ourselves and, as we take up more space on the Earth, we would look to grow those plants in increasingly hostile environments [1]. Indeed, many of the elements that make up the fertilisers we use the most to improve soil conditions are difficult to obtain or process [2]. One of the mechanisms we can use to address this is intercropping, the practice of mixing the species or genotypes of species as we plant. This can occur in time, through crop rotation which is the practice of planting different crops each season to improve soil condition. For instance, many farmers rotate planting a four crop system of brassicas, legumes, cereals, and potato plants to increase soil nutrients and ensure that certain plant-focused soil pests will die out year by year [3]. Intercropping can also occur in space, through the practice of planting different species of plants in proximity to one another to encourage a mutually beneficial relationship between them. This work will explore the benefits of intercropping in space, planting different genotypes and species of crop plants next to each other in order to study the benefits this may have upon nutrient uptake within their root systems.

One of the main nutrients plants rely upon is phosphorus (P) which is used in important processes such as cell membrane construction, DNA production, and the production of ATP [4], for an overview of the roles of P in plant growth see Figure 1. In order to maximise plant production of new cells and leaf growth it is therefore important for the plant to have a ready supply of P available in the soil [4]. For this reason, many commercial farming programs rely on P fertilisers produced from either acid- or heat-treated rock phosphate [5]. This rock phosphate is mined primarily in countries such as Morocco, China and Russia, each of which has their own political difficulties when it comes to obtaining a steady supply of resources [2]. Thus, if plants can be bred or intercropped in a certain way to more efficiently access and use the P compounds present in soil without the need of additional outside sources of P, this would be of great benefit to many farming and crop focused industries.

In this project, we will reproduce the model of zinc uptake by rice using metal-complexing phytosiderophore as an exudate [6] and extend it to model interaction of roots of two different plants growing next to each other (i.e. intercropped) with two different exudates and one common nutrient being taken from the soil. The parameters we choose to use in the model correspond to barley and tobacco plants which secrete citrate and phytase so that the plant can access P from the soil in the form of phosphate [7]. We will also experiment with different parameter set-ups and report on findings regarding the combinations of parameter values or plant traits that enhance phosphate uptake. The findings about what traits are beneficial for nutrient uptake in intercropping might be especially useful for farming focused industries as the results are not limited only to hypothetical barley and tobacco system but to any combination of plants which might satisfy the characteristics we propose.

The document is structured as follows. In Section 2, the mechanisms of zinc uptake are described and the model of [6] is introduced. In Section 3, an initial extension to two roots is discussed. A numerical scheme is also presented to solve the coupled system of nonlinear parabolic partial differential equations, it is followed by numerical experiments supported by a non-dimensionalising procedure. In Section 4, two extensions of the model are proposed for intercropping. A numerical scheme is also proposed for numerical computation, which is based on a non-dimensionalised system included in the Appendix. Parameter choice for the barley-tobacco combination and subsequent numerical experimentation of the extended model can be found in Section 5. Existence results for the coupled ordinary differential and partial differential equation systems presented in this work is delayed until Section 7, where a general approach shows the existence of a solution for all the studied models.

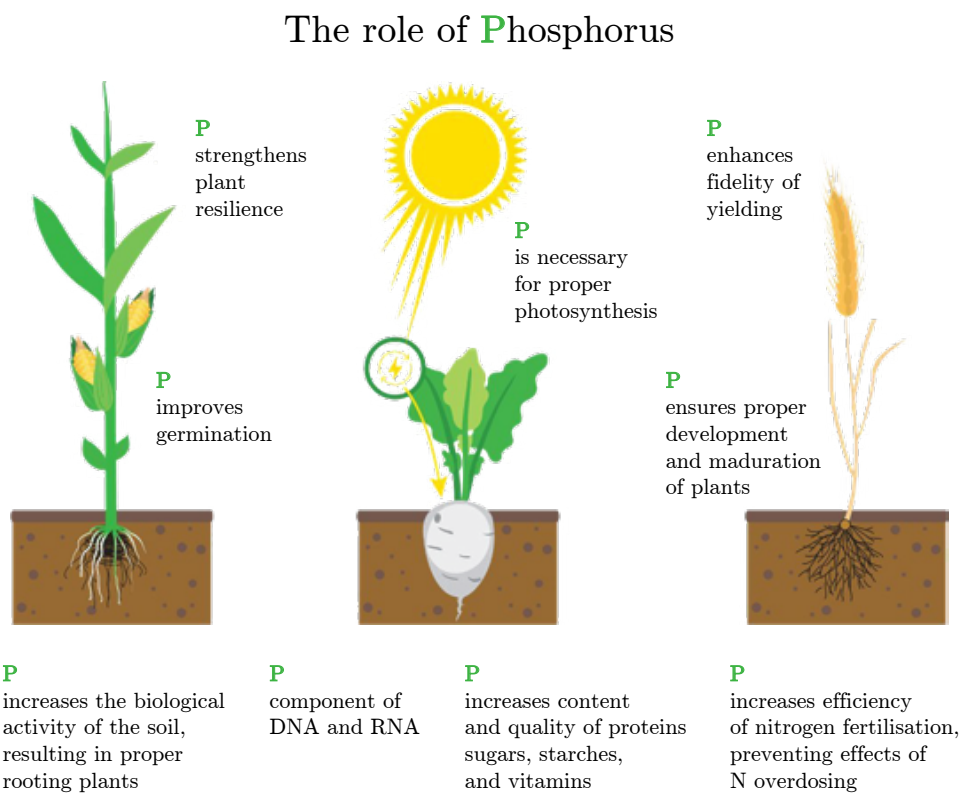

Figure 1: Phosphorus is an essential nutrient for proper growth of plants with different functions shown in the figure. Reproduced from [8].

2 Biological background and introduction to the base model

Once the motivation to this project has been established, let us introduce the plant system we are going to be working with. We introduce the reader to the biological background of the models considered in this project, along with a derivation of the base model from [6].

2.1 Dynamics at the root

In the following subsections we will briefly explain how plant roots interact with the soil around them in order to gather nutrients.

2.1.1 Root exudation and absorption

When a plant germinates from a seed, it puts roots out into the soil around and below it. For many plants, the growth of the roots results in a large system within the soil from which it can gather nutrients and water. Some root systems are made up of many first order roots which contribute equally to nutrient absorption, while others are made up of a single first order root which dominates the system, and other smaller second order roots which contribute in smaller amounts, along with root hairs. The growth of roots and root hairs can be affected by the soil environment in which the plant is growing, see Figure 2.

Each root is made up of many layers of different kinds of tissue. What is important for our model is the existence of a cell wall and membrane that nutrients must pass through to be absorbed and used by the plant for various purposes [9]. The root tip is covered by a single shell-like covering called the root cap. The root cap allows the root to push down into the soil without any important parts of its surface being damaged in the process. Because of its protective purpose, the root cap is tougher than the rest of the root [10]. In what follows, we will consider the root cap to be inactive in the processes of exudation and nutrient

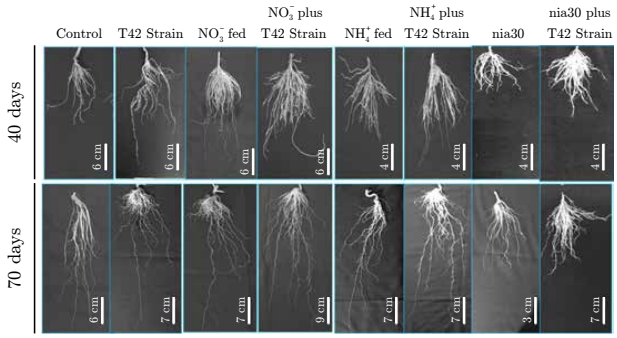

Figure 2: Different root responses to varying nutrient and moisture content in the soil, reproduced from [12].

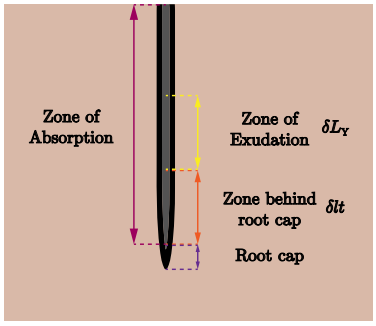

Figure 3: Diagram showing the zones of various activity on an example plant root.

uptake, and we will model only the interaction with the rest of the root. Behind the root cap, there is a zone of exudation within which the plant may secrete certain chemicals out into the soil. These chemicals may break down nutrient compounds in the soil that cannot be absorbed directly, helping the plant to utilise them. [11].

Another zone of the root important for our model is the absorption zone. In some plants, the whole root may absorb nutrients, while in others, absorption is limited to a smaller portion of the root surface. This is similar to the zone of exudation which in some plants may be very large and in others is limited to a very small region behind the root cap. This is portrayed in Figure 3 along other key zones of a sample root.

Within the absorption zone, roots absorb many different elements from the soil. While the model in [6] focuses on zinc uptake, our primary interest is the uptake of phosphorus. Both of these nutrients can be highly deficient in many soil types and interact similarly with different exudates.

2.1.2 Interaction of exudates with soil

In the case of Zn absorption, the plant exudes a phytosiderophore, deoxymugineic acid (DMA), which acts to increase the absorbtion of Zn from soils in the form of Zn^{2+} bound to soil particles, see Figure 4 for a sketch of this process. In the case of phosphorus, the interaction is a little more complex. Studies have shown that in soil with limited P availability, exudation of citrate by plant roots has improved P solubilisation in soils allowing the inorganic P to move from soil solid into solution [13]. In particular citrate, as an organic acid anion, lowers the pH of the previously neutral soil. This promotes competition in the ions that bind with metals in the soil, meaning they bind more with iron and aluminium. P strongly adsorbs to soil particle surfaces (i.e. iron and aluminium), thus with more of those bound up into other compounds, more P is free to move into solution [13]. Then we have the exudation of phytase enzymes which are responsible for the process of mineralising P, i.e. converting organic P into inorganic P, which allows the plant to utilise it. Most importantly, research has shown that working in tandem, citrate, and phytase have a much larger effect on P absorption than we can currently explain, thus we have chosen to model the exudation of both rather than taking models of each single exudate by itself [14]. The role of citrate and phytase in P absorption by the root is further explained in Figure 5.

2.2 Base model formulation

We now present the model of [6] which considers the way rice plants access Zn in Zn-deficient soils. The paper models the mechanism of DMA exudation which allows rice roots to access Zn bound to the soil particles as explained in the previous sections. Let X be the amount of the micronutrient metal Zn and Y the amount of exuded phytosiderophore DMA. All parameters following in this section are described in Table 1. The equations model the movement of X and Y by diffusion and convection through the soil pore solution, allowing for adsorption and desorption to occur on soil particle surfaces and diffusion only within

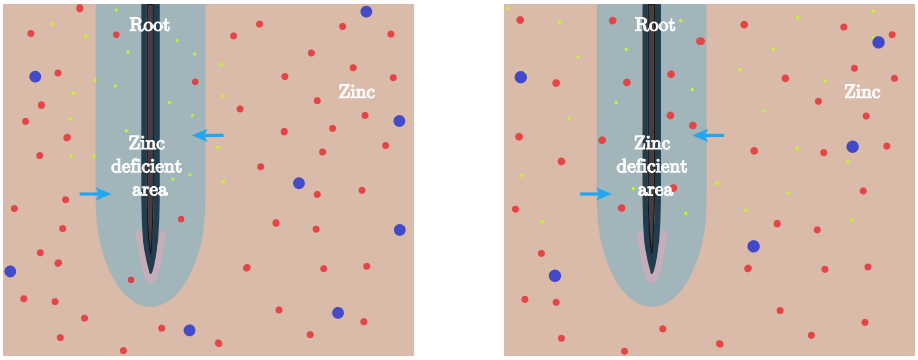

(a) (b)

Figure 4: Diagrams showing the dynamics of the exudate DMA (green) with Zn (red) in the soil; (a) DMA improves Zn solubility and then diffusion and convection effects cause it to move into the deficient area, presence of microbes which consume the DMA shown in purple; (b) after a period of time, solubilised Zn has moved into the deficient area and is more accessible to the root while some DMA particles have been consumed by microbes. Relative sizes are simply for illustrative purposes and not accurate.

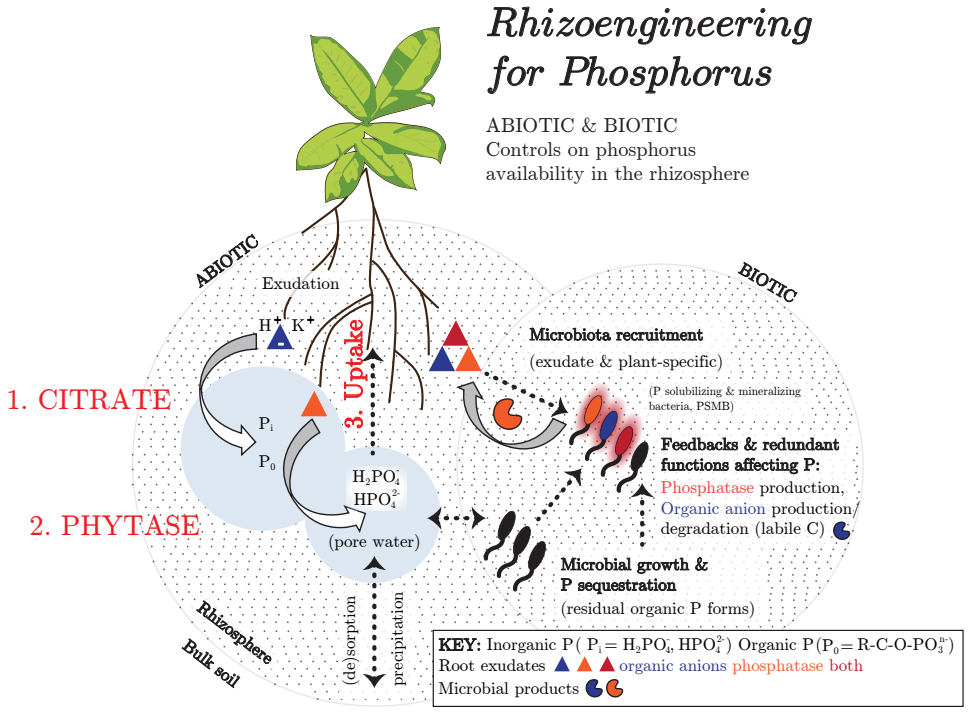

Figure 5: Role of citrate and phytase in the rhizosphere of a plant. Figure obtained by private communication with Tim George.

the soil solution. The concentrations of X and Y in the soil solution are marked by X_L and Y_L, while their concentrations in the soil solid are X_S and Y_S. Thus the conservation equations for X and Y are proposed to be

$$\begin{aligned} \partial_t(\theta X_L + X_S) &= \nabla \cdot (D_X \nabla X_L - \nu X_L) - g_X, \\ \partial_t(\theta Y_L + Y_S) &= \nabla \cdot (D_Y \nabla Y_L - \nu Y_L) - g_Y. \end{aligned} \tag{2.1}$$

We can then derive equilibrium conditions between the soil particles and solution. At equilibrium describing fast absorption and solubilisation of Zn and DMA at soil particles we have

$$\partial_t X_S = \beta_1 X_L - \beta_2 X_S - \beta_3 X_S Y_L = 0 \qquad \text{and} \qquad \partial_t Y_S = \gamma_1 Y_L - \gamma_2 Y_S - \gamma_3 Y_S X_L = 0, \tag{2.2}$$

with $\beta_1, \beta_2, \beta_3, \gamma_1, \gamma_2, \gamma_3$ being the reaction rate coefficients. By differentiating the resulting algebraic equations in (2.2) and substituting the expressions for X_S and Y_S into the system (2.1), we obtain the reduced system of parabolic equations

$$\left(\theta + \frac{b_X}{1+\kappa_X b_X Y_L}\right)\partial_t X_L - \frac{\kappa_X b_X^2 X_L}{(1+\kappa_X b_X Y_L)^2}\partial_t Y_L = \nabla\cdot(D_X \nabla X_L - \nu X_L) - g_X, \tag{2.3a}$$

$$\left(\theta + \frac{b_Y}{1+\kappa_Y b_Y X_L}\right)\partial_t Y_L - \frac{\kappa_Y b_Y^2 Y_L}{(1+\kappa_Y b_Y X_L)^2}\partial_t X_L = \nabla\cdot(D_Y \nabla Y_L - \nu Y_L) - g_Y. \tag{2.3b}$$

Having derived the dynamics of X_L and Y_L in soil, we will now insert a plant root into the system by determining boundary conditions of our domain. The concentrations of X_L and Y_L depend upon the pair of spatial variables in $(r, z) \in \mathbb{R}^2$ which measure radial distance from the center of the root and length from the soil surface respectively as shown in Figure 6, respectively. Furthermore, we specify the domain by restricting to $r \in [a, x]$ where a is the diameter of the root and x is radius of zone of root influence. Notice that we are modelling the region starting at the surface of the root and the root itself is not part of the domain. In the vertical direction, we will restrict to $z \in [-L_{t_{\max}}, 0]$ as we assume the root growing into the downward direction, reaching length of the active zone of the root $L_{t_{\max}}$ at the end of simulation at some time $t_{\max}$. We note that we consider the active zone of the root to be the zone up to where the root cap begins, see Figure 3. The presence of a single plant root on one vertical edge (on the left-hand side of the domain) results in

$$D_X \partial_r X_L - \nu X_L = \alpha X_L \qquad \text{at } r = a, \quad z \in [-L, -(L - \delta L_X)], \tag{2.3c}$$

$$D_Y \partial_r Y_L - \nu Y_L = -F_Y(t) \qquad \text{at } r = a, \quad z \in [-(L - \delta lt), -(L - \delta lt - \delta L_Y)]. \tag{2.3d}$$

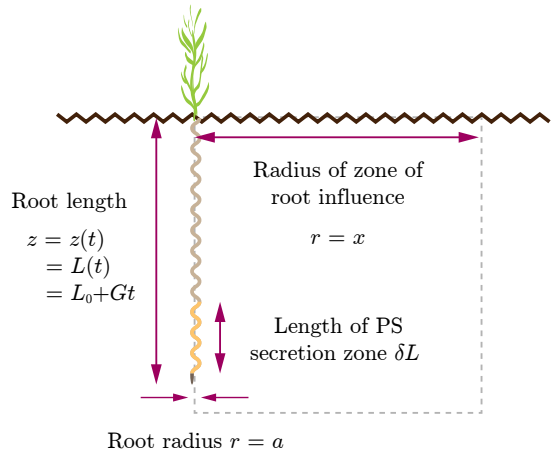

Figure 6: Sketch of the domain for system with one plant as modelled in [6] with L_0 being the length of root at the beginning of simulation and G being the growth rate of the root. The root portrayed is curly for illustration purposes.

For the rest of the boundary, we have zero-flux conditions; i.e., in the case of the other edge $r = x$, this is just

$$D_X \partial_r X_L - \nu X_L = 0 \qquad \text{and} \qquad D_Y \partial_r Y_L - \nu Y_L = 0. \tag{2.3e}$$

Boundary condition (2.3d) represents the exudation of DMA from a region on the root surface of length δL_Y located at distance δlt behind the end of root cap, while the absorption of Zn from the soil surrounding the root is captured by (2.3c) at region of length δL_X behind the start of root cap. In all the simulations in this report we will assume nutrient absorption along the whole root except the root cap, i.e. $\delta L_X = L$, but keep the interval for absorption in the general form as above. Although the exudation rate $F_Y(t)$ was initially

modelled to be dependent of time, the conclusions of the original paper allow us to eventually keep it as a constant over 24 hours. For the simulations in this report, we will consider there is no exudate Y_L in the rhizosphere, i.e. $Y_L = Y_L^0 = 0$ at $t = 0$, and the initial condition for the nutrient, $X_L = X_L^0$ at $t = 0$, will be set according to the nutrient and specified in the sections for numerical experiments. We will also assume that the simulations start when the active part of the root is 5 cm long, i.e. $L_0 = 0.5$ dm.

Symbol	Meaning
θ	Solution volume fraction
f	Diffusion impedance factor
$D_{L,X}$	Diffusion coefficient of nutrient X in free solution
$D_{L,Y}$	Diffusion coefficient of exudate Y in free solution
D_X	Diffusion of the the nutrient X in the soil, $D_X = D_{L,X}\theta f$
D_Y	Diffusion of the exudate Y in the soil, $D_Y = D_{L,Y}\theta f$
ν	Water flux
g_X	Function for the immobilisation of nutrient X
g_Y	Function for decomposition of the exudate Y
b_X	Buffer power of X
b_Y	Buffer power of Y
κ_X	X - Y interaction coefficient
κ_Y	Y - X interaction coefficient
α	X-absorbing power of root
F_Y	Rate of Y exudation
L	Length of root at certain time, increases at rate G
δL_X	Length of X uptake zone
δL_Y	Length of Y exudation zone
δlt	Length of the zone between the end of exudation zone and the beginning of root cap
a	Root radius
x	Radius of zone of root influence

Table 1: Table of parameters and their meanings for the base model.

3 Base model extension

In this section, we will continue studying the original model from [6]. First, we extend the model to include two roots secreting an exudate Y in order to facilitate absorption of a nutrient X from the soil. Second, a non-dimensionalisation procedure is presented. Third, a numerical approach is discussed to approximate solutions of the coupled partial differential equation systems. Finally, we finish with a set of numerical simulations for the two roots model.

3.1 Extension to two roots

We can extend model (2.3) by applying symmetry in the boundary conditions to consider another root in the domain, see Figure 7. Since we are not making any changes to the system itself, we are still limited to modelling one exudate and nutrient being absorbed. Nonetheless, the generalisation of the boundary conditions allow us to adjust the characteristics of the second root, namely the uptake power, exudation rate, growth rate, and exudation and uptake zones at the root. The extended set of boundary conditions is

$$D_X\partial_r X_L - \nu X_L = \alpha_1 X_L \qquad \text{at } r = a, \qquad z \in [-L_1, -(L_1 - \delta L_{X,1})], \tag{3.1a}$$

$$D_Y\partial_r Y_L - \nu Y_L = -F_{Y,1}(t) \qquad \text{at } r = a, \qquad z \in [-(L_1 - \delta lt_1), -(L_1 - \delta lt_1 - \delta L_{Y,1})], \tag{3.1b}$$

$$D_X\partial_r X_L - \nu X_L = -\alpha_2 X_L \qquad \text{at } r = w + a, \qquad z \in [-L_2, -(L_2 - \delta L_{X,2})], \tag{3.1c}$$

$$D_Y \partial_r Y_L - \nu Y_L = F_{Y,2}(t) \qquad \text{at } r = w + a, \qquad z \in [-(L_2 - \delta l t_2), -(L_2 - \delta l t_2 - \delta L_{Y,2})], \tag{3.1d}$$

where the parameters bear the same meanings as in Table 1, and they are indexed by the root they correspond to; i.e. 1 for the left-hand side of the domain and 2 for the right-hand side of the domain. We note that in this general setting the two plants can have different growth rates, i.e. $L_1 = L_{0,1} + G_1 t$, $L_2 = L_{0,2} + G_2 t$, where $L_{0,1}$, $L_{0,2}$ are root lengths at the beginning of the simulation. However, in the numerical experiment in this section we choose to model both roots with the same set of parameters as in [6]. The second root is located at $r = w + a$ where w is the width of the space between the two roots. This distance can be manipulated so that the zones of root influence intersect with each other; thus allowing to model intercropping and the effect of the proximity of two roots on each other. For the rest of the boundary we consider zero-flux boundary conditions.

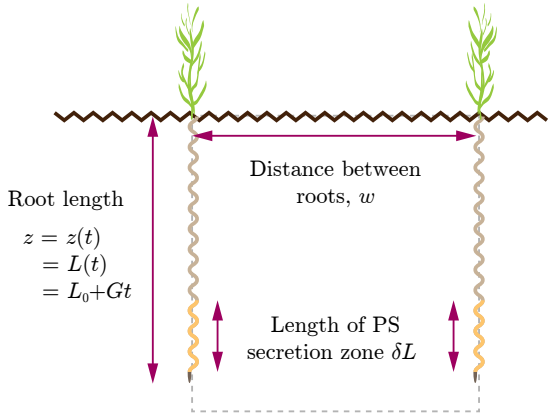

Figure 7: Sketch of the domain for system with two plants and one exudate.

3.2 Non-dimensionalisation

As a standard procedure, we will non-dimensionalise the variables of model (3.1). For this end, we introduce the following relations

$$r = \varepsilon_r \hat{r} + a, \qquad z = \varepsilon_z \hat{z}, \qquad t = \varepsilon_t \hat{t}, \qquad X_L = \varepsilon_x \hat{x}, \qquad Y_L = \varepsilon_y \hat{y};$$

where $\varepsilon_r, \varepsilon_z, \varepsilon_t, \varepsilon_x, \varepsilon_y$ are scaling constants to be determined, and $\hat{r}, \hat{z}, \hat{t}, \hat{x}, \hat{y}$ are non-dimensional variables. Clearly, we have the relation $X_L(r,z) = \varepsilon_x \hat{x}(\varepsilon_r \hat{r} + a, \varepsilon_z \hat{z}) = \varepsilon_x \hat{x}\left(\varepsilon_r^{-1}(r-a), \varepsilon_z^{-1} z\right)$ and similarly $Y_L(r,z) = \varepsilon_y \hat{y}\left(\varepsilon_r^{-1}(r-a), \varepsilon_z^{-1} z\right)$. Using this, we see that the gradient operator is also scaled as

$$\nabla X_L = \begin{pmatrix} 1/\varepsilon_r & 0 \\ 0 & 1/\varepsilon_z \end{pmatrix} \hat{\nabla} \varepsilon_x \hat{x}, \qquad \text{with} \qquad \hat{\nabla} = \begin{pmatrix} \frac{\partial}{\partial \hat{r}} & \frac{\partial}{\partial \hat{z}} \end{pmatrix}^\top.$$

For the left-hand side of (2.3a) we have that

$$\left(\theta + \frac{b_X}{1 + \kappa_X b_X Y_L}\right) \partial_t X_L = \frac{\varepsilon_x}{\varepsilon_t} \left(\theta + \frac{b_X}{1 + \varepsilon_y \kappa_X b_X \hat{y}}\right) \frac{\partial \hat{x}}{\partial \hat{t}} \tag{3.2}$$

$$-\frac{\kappa_X b_X^2 X_L}{(1 + \kappa_X b_X Y_L)^2} \partial_t Y_L = -\frac{\varepsilon_x}{\varepsilon_t} \frac{\varepsilon_y \kappa_X b_X^2 \hat{x}}{(1 + \varepsilon_y \kappa_X b_X \hat{y})^2} \frac{\partial \hat{y}}{\partial \hat{t}} \tag{3.3}$$

The right-hand side requires some care. We introduce the non-dimensional quantities $\hat{v}_r$ and $\hat{v}_z$ such that $\nu = {}^{\varepsilon_r}/_{\varepsilon_t}\hat{v}_r$ and $\nu = {}^{\varepsilon_z}/_{\varepsilon_t}\hat{v}_z$, and $\hat{D}_{X,r}$ and $\hat{D}_{X,z}$ such that $D_X = {}^{\varepsilon_r^2}/_{\varepsilon_t}\hat{D}_{X,r}$ and $D_X = {}^{\varepsilon_z^2}/_{\varepsilon_t}\hat{D}_{X,z}$. This way, we have that

$$\begin{aligned}\nabla \cdot (D_X \nabla X_L - \nu X_L) &= \begin{pmatrix} {}^{1}/_{\varepsilon_r} & 0 \\ 0 & {}^{1}/_{\varepsilon_z} \end{pmatrix} \hat{\nabla} \cdot \left(D_X \varepsilon_x \begin{pmatrix} {}^{1}/_{\varepsilon_r} & 0 \\ 0 & {}^{1}/_{\varepsilon_z} \end{pmatrix} \hat{\nabla}\hat{x} - \nu\varepsilon_x \hat{x} \right) \\ &= \frac{\varepsilon_x}{\varepsilon_t} \hat{\nabla} \cdot \left(\begin{pmatrix} \hat{D}_{X,r} & 0 \\ 0 & \hat{D}_{X,z} \end{pmatrix} \hat{\nabla}\hat{x} - \hat{x} \begin{pmatrix} \hat{v}_r \\ \hat{v}_z \end{pmatrix} \right). \end{aligned} \tag{3.4}$$

For g_X we introduce the non-dimensional quantity $\frac{\varepsilon_x}{\varepsilon_t}\hat{g}_x = g_X$. Equation (2.3b) and the parameters involved follow a similar argument.

3.2.1 Boundary and initial conditions

Let us now discuss the non-dimensionalisation of the boundary conditions. For the one-root model (2.3), we have that (3.1a) is equivalent to

$$D_X \partial_r X_L - \nu X_L = \frac{\varepsilon_r^2}{\varepsilon_t}\hat{D}_{X,r}\frac{\varepsilon_x}{\varepsilon_r}\frac{\partial \hat{x}}{\partial \hat{r}} - \frac{\varepsilon_r}{\varepsilon_t}\hat{v}_r\varepsilon_x\hat{x} = \frac{\varepsilon_r\varepsilon_x}{\varepsilon_t}\hat{\alpha}_1\hat{x} \qquad \text{at } r = a = a + \varepsilon_r\hat{r}, \quad \varepsilon_z\hat{z} \in [-L_1, -(L_1 - \delta L_{X,1})],$$

or equivalently

$$\hat{D}_{X,r}\frac{\partial \hat{x}}{\partial \hat{r}} - \hat{v}_r\hat{x} = \hat{\alpha}_1\hat{x} \qquad \text{at } \hat{r} = 0, \quad \hat{z} \in [-\hat{L}_1, -(\hat{L}_1 - \delta\hat{L}_{x,1})]; \tag{3.5}$$

where we require $\alpha_1 = {}^{\varepsilon_r}/_{\varepsilon_t}\hat{\alpha}_1$, $\hat{L}_1 = \varepsilon_z^{-1}L_1$, and $\delta\hat{L}_{x,1} = \varepsilon_z^{-1}\delta L_{X,1}$. Likewise for (3.1b), we get

$$\hat{D}_{Y,r}\frac{\partial \hat{y}}{\partial \hat{r}} - \hat{v}_r\hat{y} = -\hat{F}_{y,1}(t) \qquad \text{at } \hat{r} = 0, \quad \hat{z} \in [-(\hat{L}_1 - \delta\widehat{lt}_1), -(\hat{L}_1 - \delta\widehat{lt}_1 - \delta\hat{L}_{y,1})]. \tag{3.6}$$

Finally, conditions (3.1c) and (3.1d) are just

$$\hat{D}_{X,r}\frac{\partial \hat{x}}{\partial \hat{r}} - \hat{v}_r\hat{x} = \hat{\alpha}_2\hat{x} \qquad \text{at } \hat{r} = \frac{w}{\varepsilon_r}, \quad \hat{z} \in [-\hat{L}_2, -(\hat{L}_2 - \delta\hat{L}_{x,2})], \tag{3.7a}$$

$$\hat{D}_{Y,r}\frac{\partial \hat{y}}{\partial \hat{r}} - \hat{v}_r\hat{y} = -\hat{F}_{y,2}(t) \qquad \text{at } \hat{r} = \frac{w}{\varepsilon_r}, \quad \hat{z} \in [-(\hat{L}_2 - \delta\widehat{lt}_2), -(\hat{L}_2 - \delta\widehat{lt}_2 - \delta\hat{L}_{y,2})]. \tag{3.7b}$$

Conditions (3.5) and (3.7) give us a hint of how we need to select ε_r and ε_z. If we select $\varepsilon_r = w$, then $\hat{r}$ will be in the range $[0, 1]$. Similarly, if we pick $\varepsilon_z = \max\{L_{t_{\max},1}, L_{t_{\max},2}\}$, again $\hat{z}$ will be in the range $[0, -1]$. This last selection implies that the maximum absolute value of $\hat{L}$ should be 1 where we have

$$\hat{L}_i = \hat{L}_i(\hat{t}) = \frac{1}{\varepsilon_z}(L_{0,i} + G_i\varepsilon_t\hat{t}) = \hat{L}_{0,i} + \hat{G}\hat{t}, \qquad \hat{L}_{0,i} = \varepsilon_z^{-1}L_{0,i}, \qquad \hat{G}_i = \varepsilon_t\varepsilon_z^{-1}G_i,$$

for $i \in \{1, 2\}$. Furthermore, we can further select $\varepsilon_t = t_{\max}$ to finally have $\hat{t}$ in the range $[0, 1]$.

Notice that we have selected scaling parameters such that the system of partial differential equations is defined in $[0, 1] \times [0, -1] \times [0, 1]$. We will denote the scaled spatial domain as $\Omega := [0, 1] \times [0, -1]$ and its boundary $\Gamma := \partial\Omega$. Lastly, the initial conditions are scaled as $(\hat{x}_0, \hat{y}_0) = (\varepsilon_x^{-1}X_L^0, \varepsilon_y^{-1}Y_L^0)$.

3.3 Numerical approximation scheme

In order to get numerical solutions of the coupled system of partial differential equations (2.3a)–(2.3b) with boundary conditions (2.3c)–(2.3d) or (3.1), we will use a decoupling scheme by linearisation. Defining $u := (\hat{x}, \hat{y})$, we aim to solve a system of the form $\frac{\partial \hat{x}}{\partial \hat{t}} = A_1(u)$, $\frac{\partial \hat{y}}{\partial \hat{t}} = A_2(u)$ with $u(0) = u_0$. An approach, as shown in [15], is to select the operators A_1 and A_2 such that we solve a linear system of PDEs for $\hat{y}$ and then a subsequent linear system of PDEs for $\hat{x}$.

The general approach is as follows. We start discretising the time domain with steps of length $\Delta\hat{t}$. At step $m = 0$, we solve the reduced problem $\frac{\partial \hat{y}}{\partial \hat{t}} = \tilde{A}_1(\hat{x}^m, \hat{y}; \hat{y}^m)$ with $\hat{y}(m\Delta\hat{t}) = \hat{y}^m$, and $t \in [m\Delta\hat{t}, (m+1)\Delta\hat{t}]$. Here $\tilde{A}_1(\hat{x}^m, \hat{y}; \hat{y}^m)$ indicates that nonlinearities in A_1 are evaluated at $\hat{x}^m$ and $\hat{y}^m$ such that the resulting differential operator is linear in $\hat{y}$. The solution, labelled $\hat{y}^{m+1}$, is then used to solve $\frac{\partial \hat{x}}{\partial \hat{t}} = \tilde{A}_2(\hat{x}, \hat{y}^{m+1}; \hat{x}^m)$ with $\hat{x}(m\Delta\hat{t}) = \hat{x}^m$, and $t \in [m\Delta\hat{t}, (m+1)\Delta\hat{t}]$. Then we repeat the process for the next steps.

Additionally, we will approximate the time derivatives using simple backward differences. The explicit form of the resulting numerical scheme will be presented using a variational expression defined over the spatial domain Ω.

3.3.1 Non-dimensionalised variational expressions

The existence of a solution to the model (2.3) with boundary conditions (3.1) is presented in Section 7. For now, let us suppose that there is a sufficiently smooth solution pair $(\hat{x}, \hat{y})$ for each time $\hat{t} \in [0, 1]$. Now, let us fix $\hat{t} \in (0, 1)$. We introduce the nonlinear terms

$$A(\hat{y}) = \theta + \frac{b_X}{1 + \hat{\kappa}_X b_X \hat{y}}, \qquad B(\hat{x}, \hat{y}) = \frac{\hat{\kappa}_X b_X^2 \hat{x}}{(1 + \hat{\kappa}_X b_X \hat{y})^2}, \tag{3.8}$$

$$C(\hat{x}) = \theta + \frac{b_Y}{1 + \hat{\kappa}_Y b_Y \hat{x}}, \qquad E(\hat{x}, \hat{y}) = \frac{\hat{\kappa}_Y b_Y^2 \hat{y}}{(1 + \hat{\kappa}_Y b_Y \hat{x})^2}; \tag{3.9}$$

where we have used the scaled constants $\hat{\kappa}_X = \varepsilon_y \kappa_X$, $\hat{\kappa}_Y = \varepsilon_x \kappa_Y$.

Multiply the scaled equations of the parabolic system by two $v_a, v_b \in \mathcal{C}^1(\bar{\Omega})$ functions and integrate this with respect to the pair (r, z) using the Lebesgue measure μ. Using the Divergence Theorem [16], we have

$$\begin{aligned}
\int_\Omega A(\hat{y}) \frac{\partial \hat{x}}{\partial \hat{t}} v_a - B(\hat{x}, \hat{y}) \frac{\partial \hat{y}}{\partial \hat{t}} v_a \, \mathrm{d}\mu &= \int_\Omega \left(\hat{x}\hat{v} - \hat{D}_x \hat{\nabla} \hat{x} \right) \cdot \hat{\nabla} v_a - \hat{g}_x v \, \mathrm{d}\mu + \int_\Gamma \left(\hat{D}_x \hat{\nabla} \hat{x} - \hat{x}\hat{v} \right) \cdot \vec{n} v_a \, \mathrm{d}\sigma, \\
\int_\Omega C(\hat{x}) \frac{\partial \hat{y}}{\partial \hat{t}} v_b - E(\hat{x}, \hat{y}) \frac{\partial \hat{x}}{\partial \hat{t}} v_b \, \mathrm{d}\mu &= \int_\Omega \left(\hat{y}\hat{v} - \hat{D}_y \hat{\nabla} \hat{y} \right) \cdot \hat{\nabla} v_b - \hat{g}_y v_b \, \mathrm{d}\mu + \int_\Gamma \left(\hat{D}_y \hat{\nabla} \hat{y} - \hat{y}\hat{v} \right) \cdot \vec{n} v_b \, \mathrm{d}\sigma;
\end{aligned} \tag{3.10}$$

where Γ is the boundary of Ω, $\vec{n}$ its normal vector, and σ the surface measure on Γ. The resulting equations for the extended model (3.1) yield

$$\begin{aligned}
\int_\Omega A(\hat{y}) \frac{\partial \hat{x}}{\partial \hat{t}} v_a - B(\hat{x}, \hat{y}) \frac{\partial \hat{y}}{\partial \hat{t}} v_a \, \mathrm{d}\mu &= \int_\Omega \left(\hat{x}\hat{v} - \hat{D}_x \hat{\nabla} \hat{x} \right) \cdot \hat{\nabla} v_a - \hat{g}_x v_a \, \mathrm{d}\mu - \int_{\Gamma_{1,x}} \hat{\alpha}_1 \hat{x} v_a \, \mathrm{d}\sigma - \int_{\Gamma_{2,x}} \hat{\alpha}_2 \hat{x} v_a \, \mathrm{d}\sigma, \\
\int_\Omega C(\hat{x}) \frac{\partial \hat{y}}{\partial \hat{t}} v_b - E(\hat{x}, \hat{y}) \frac{\partial \hat{x}}{\partial \hat{t}} v_b \, \mathrm{d}\mu &= \int_\Omega \left(\hat{y}\hat{v} - \hat{D}_y \hat{\nabla} \hat{y} \right) \cdot \hat{\nabla} v_b - \hat{g}_y v \, \mathrm{d}\mu + \int_{\Gamma_{1,y}} \hat{F}_{y,1} v_b \, \mathrm{d}\sigma + \int_{\Gamma_{2,y}} \hat{F}_{y,2} v_b \, \mathrm{d}\sigma.
\end{aligned} \tag{3.11}$$

Here we have two segments for each root at time $\hat{t}$. For the first, there are $\Gamma_{1,x} = \{0\} \times [-\hat{L}_1, -(\hat{L}_1 - \delta\hat{L}_{x,1})]$ and $\Gamma_{1,y} = \{0\} \times [-(\hat{L}_1 - \delta\widehat{lt}_1), -(\hat{L}_1 - \delta\widehat{lt}_1 - \delta\hat{L}_{y,1})]$. While for the second, we have $\Gamma_{2,x} = \{1\} \times [-\hat{L}_2, -(\hat{L}_2 - \delta\hat{L}_{x,2})]$ and $\Gamma_{2,y} = \{1\} \times [-(\hat{L}_2 - \delta\widehat{lt}_2), -(\hat{L}_2 - \delta\widehat{lt}_2 - \delta\hat{L}_{y,2})]$. Notice that they depend on the

current time $\hat{t}$.

Observe that (3.11) holds, by density, for any $v_a, v_b \in H^1(\Omega)$. This assumes that $\hat{x}$ and $\hat{y}$, and their corresponding time derivatives, are defined pointwise in time.

3.3.2 Time discretisation and decoupling

As we mentioned before, we use a simple backward difference to approximate the time derivative. To do this, we discretise the time domain by $N+1$ uniform steps of length $\Delta\hat{t}$. Here, let the superscript n denote a quantity at time $\hat{t}_n$, where n is an integer counting time levels, e.g. $\hat{x}^n$ is $\hat{x}$ evaluated at time level n. This yields

$$\left(\frac{\partial \hat{x}}{\partial \hat{t}}\right)^{n+1} \approx \frac{\hat{x}^{n+1} - \hat{x}^n}{\Delta \hat{t}} \tag{3.12}$$

for all $n \in \{0, \dots, N\}$.

Inserting this in the variational system, and applying the splitting technique discussed for (**??**), we get that the extension for two roots with boundary conditions (3.1) is approximated by the following scheme. Initialising $\hat{x}^0 = \hat{x}^{-1} = \hat{x}_0$ and $\hat{y}^0 = \hat{y}_0$, then for every $n \in \{0, \dots, N\}$: (A) Solve the variational problem of finding $\hat{y}^{n+1}$ such that

$$\begin{aligned} &\int_\Omega C(\hat{x}^n)(\hat{y}^{n+1} - \hat{y}^n)v - E(\hat{x}^n, \hat{y}^{n+1})(\hat{x}^n - \hat{x}^{n-1})v \,\mathrm{d}\mu \\ &\qquad = \Delta\hat{t}\Bigg(\int_\Omega \left(\hat{y}^{n+1}\hat{v} - \hat{D}_y \hat{\nabla}\hat{y}^{n+1}\right) \cdot \hat{\nabla} v \,\mathrm{d}\mu - \int_\Omega \hat{g}_y^n v \,\mathrm{d}\mu + \int_{\Gamma_{1,y}^{n+1}} \hat{F}_{y,1} v \,\mathrm{d}\sigma + \int_{\Gamma_{2,y}^{n+1}} \hat{F}_{y,2} v \,\mathrm{d}\sigma \Bigg) \end{aligned} \tag{3.13a}$$

for every $v \in H^1(\Omega)$. (B) Proceed on finding $\hat{x}^{n+1}$ such that it satisfies

$$\begin{aligned} &\int_\Omega A(\hat{y}^n)(\hat{x}^{n+1} - \hat{x}^n)v - B(\hat{x}^{n+1}, \hat{y}^n)(\hat{y}^{n+1} - \hat{y}^n)v \,\mathrm{d}\mu \\ &\qquad = \Delta\hat{t}\Bigg(\int_\Omega \left(\hat{x}^{n+1}\hat{v} - \hat{D}_x \hat{\nabla}\hat{x}^{n+1}\right) \cdot \hat{\nabla} v \,\mathrm{d}\mu - \int_\Omega \hat{g}_x^n v \,\mathrm{d}\mu - \int_{\Gamma_{1,x}^{n+1}} \hat{\alpha}_1 \hat{x}^{n+1} v \,\mathrm{d}\sigma - \int_{\Gamma_{2,x}^{n+1}} \hat{\alpha}_2 \hat{x}^{n+1} v \,\mathrm{d}\sigma \Bigg) \end{aligned} \tag{3.13b}$$

for every $v \in H^1(\Omega)$.

In the approximation scheme, each contributing subset of Γ is updated for the current time step. For instance, segment $\Gamma_{1,y}^{n+1}$ is the segment $\Gamma_{1,y}$ at time $\hat{t}_{n+1} = (n+1)\Delta\hat{t}$.

3.3.3 Implementation comments

The variational problems in (3.13) will be solved using FEniCS [17] with its Python interface. FEniCS is a framework for PDE modeling, continuum mechanics, and physics simulations, and it enables users to translate the mathematical problem into Python code and solve it efficiently using the finite element method [18]. The main benefits of this software are that the code is close to the mathematical formulation and that the implementation of the model does not get much more difficult as the complexity of the model increases. The code and related files are available in the repository of this project as mentioned in Appendix A.

In FEniCS, we define the boundaries as the edges of the rectangular domain. However, neither of our boundary conditions is valid on the whole edge but only on a part of it (along the whole root or a segment). Let us first consider the original model from [6] in its non-dimensionalised version, which is identical to

the one derived above. Here the segments Γ_x and Γ_y are defined by indicator functions. The first indicator function should attain value one along the whole root except the root cap (i.e. where the uptake of a nutrient happens). Thus, the indicator function should act on the interval $0 \geq \hat{z} \geq -(\hat{L}_0 + \hat{G}\hat{t})$, as the root is growing downwards. We would prefer for the indicator function to not be a step function as its discontinuity is likely to cause numerical issues. Therefore, we opt for an arctan regularisation of the form

$$I_1(\hat{z}) = \frac{1}{\pi} \arctan\left(c\Big(\hat{z} + (\hat{L}_0 + \hat{G}\hat{t})\Big)\right) + \frac{1}{2}, \tag{3.14}$$

where c defines the steepness of the regularisation. The multiplication by $\frac{1}{\pi}$ and addition of $\frac{1}{2}$ sets the range of the function from 0 to 1 in the sense of $\lim_{\hat{z}\to\infty} I_1(\hat{z}) = 1$ and $\lim_{\hat{z}\to-\infty} I_1(\hat{z}) = 0$.

The second indicator function is for the exudation boundary condition at $-(\hat{L}_0 + \hat{G}\hat{t} - \delta\widehat{lt} - \delta\hat{L}_y) \geq z \geq -(\hat{L}_0 + \hat{G}\hat{t} - \delta\widehat{lt})$. Again, we use a similar regularisation

$$I_2(\hat{z}) = \frac{1}{\pi}\left[\arctan\left(c\Big(\hat{z} + (\hat{L}_0 + \hat{G}\hat{t} - \delta\widehat{lt})\Big)\right) - \arctan\left(c\Big(\hat{z} + (\hat{L}_0 + \hat{G}\hat{t} - \delta\widehat{lt} - \delta\hat{L}_Y)\Big)\right)\right]. \tag{3.15}$$

The regularised indicators $I_1(\hat{z})$, $I_2(\hat{z})$ can be mirrored easily to act on the second root in the system as their values do not depend on the $\hat{r}$ coordinate, with their parameters possibly adjusted to change the characteristics of the root as described in Section 3.1.

3.4 Numerical experiments

Using parameters from Table 1 in [6], we can experiment with the proximity of two rice plants in the two-root model, their exudation rate and uptake power.

3.4.1 Benchmark result

For the benchmark solution we choose parameters as in [6] and run the model with both roots having the same characteristics. Our domain is symmetrical with one root on either side with equal parameters. This is evident as shown in Figure 8c which plots the cumulative Zn uptake over 24 hours. The concentrations of DMA and Zn in the soil solution after 24 hours can be found in Figure 8a and 8b, respectively. We show the final frames after 24 hours to give a snapshot of the results after a significant period of time. As we can see in this base model we observe a good amount of cooperation occurring between the two roots. The DMA exuded from the left root has diffused in the direction of the root on the right and vice versa, which is causing more Zn to be made available to both roots. Since the domain is symmetric and the roots are placed so that their zones of root influence intersect, interaction of this sort between the two roots was expected. Thus it is intuitive to consider what happens when the roots are moved further apart and whether this band of increased Zn concentration is maintained over distance.

3.4.2 Increased distance between roots

Now that the roots have been planted so that their rhizospheres are separated by a large amount of soil area, we can observe they have a weaker effect upon each other. In Figure 9a we see that the areas with increased DMA concentrations at each root no longer meet in between the roots. Figure 9b showing Zn concentration also reflects this, there is no longer a central band of accessible Zn within the soil, instead we see two separate zones of increased Zn concentration, perhaps connected very weakly even at this distance as is shown in the very slight band of yellowing within the green area of the soil.

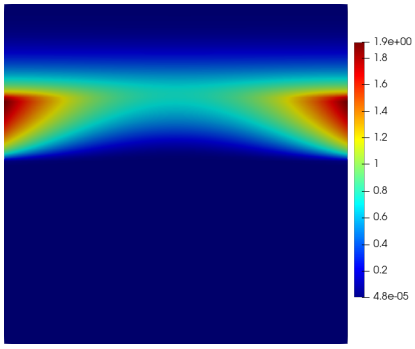

(a) DMA

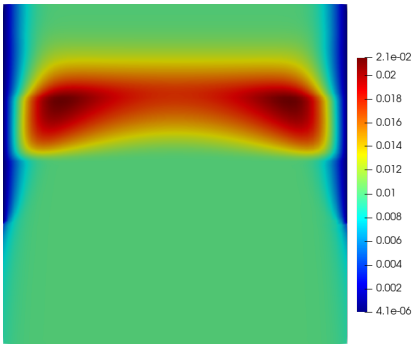

(b) Zn

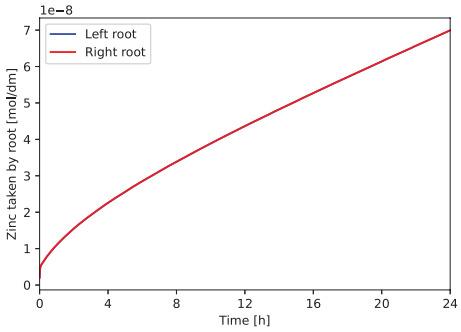

(c) Cumulative Zn uptake by the left (L) and right (R) root

Figure 8: Base model with parameters from [6] applied to both roots, with $w = 0.08$ dm. In (a) concentration of DMA and (b) concentration of Zn after 24 hours in µM; (c) the amount of Zn absorbed by each root is the same.

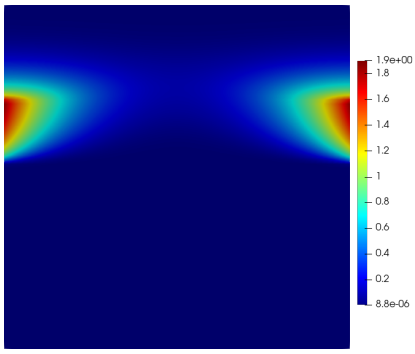

(a) DMA

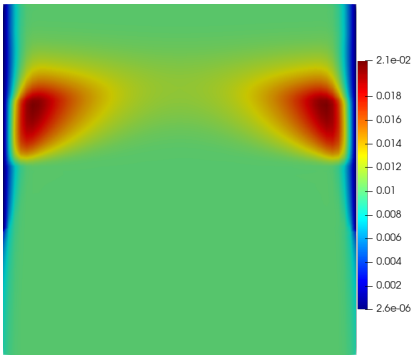

(b) Zn

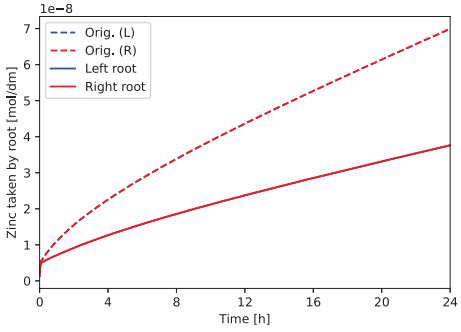

(c) Cumulative Zn uptake by the left (L) and right (R) root

Figure 9: Root distance increased to $w = 0.15$ dm. In (a) concentration of DMA and (b) concentration of Zn after 24 hours in µM; (c) the amount of Zn absorbed by each root has decreased compared to setup with $w = 0.08$ dm.

3.4.3 Increased DMA exudation

With a larger exudation rate of DMA by the plants, F_Y, we see a larger amount of Zn in the soil as could be intuitively expected. The bands we see in Figure 10a and 10b are larger and more concentrated in these conditions compared to the benchmark solution, which resulted in more Zn absorbed by the root as is shown in Figure 10c. This suggests that rice plants with a stronger expression of the genes linked with DMA exudation may be better at accessing Zn in soil and leads us to question whether they would allow an increased distance between plants before this positive cooperation would fade, which can be investigated further.

3.4.4 Increased distance between roots and DMA exudation rate

The comparison of Zn uptake at $w = 0.15$ dm with original (dashed line) and increased (solid line) exudation rate is shown in Figure 11c. We see that at this distance, the root absorbs more Zn when the exudation rate is larger. In Figure 11b we see that more Zn is available to each plant. The amount of Zn absorbed is still not as large as in the benchmark result with roots closer together. An examination of the relationship between a suitable exudation rate and root proximity to achieve a desired amount of Zn absorbed by the root would be interesting in future work. Of course, this would have to allow for the total amount of Zn in the soil as a limiting factor, keeping in mind realistic limits on the amount of DMA possible for the plants to exude.

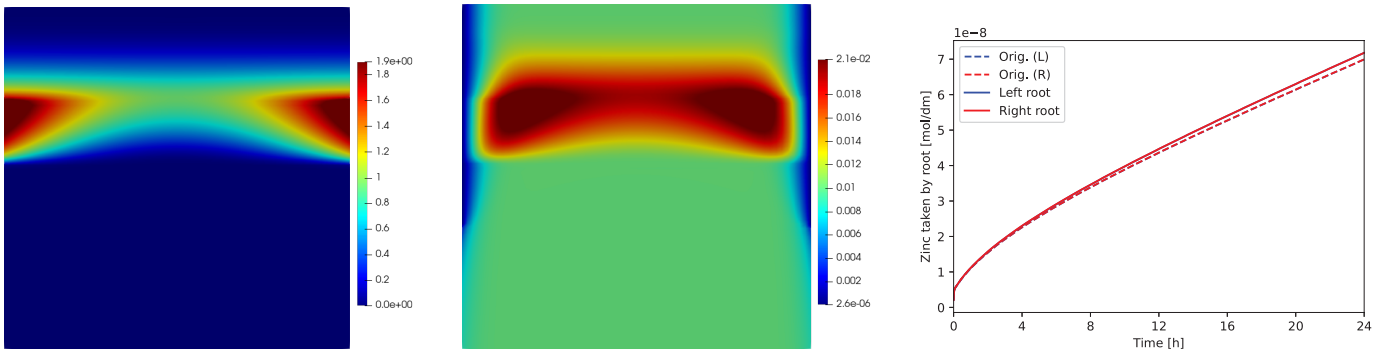

(a) DMA (b) Zn (c) Cumulative Zn uptake by the left (L) and right (R) root

Figure 10: DMA exudation rate F_Y increased by 10^{-11}. In (a) concentration of DMA and (b) concentration of Zn after 24 hours in µM; (c) the amount of Zn absorbed by each root has increased compared to uptake with the original exudation rate.

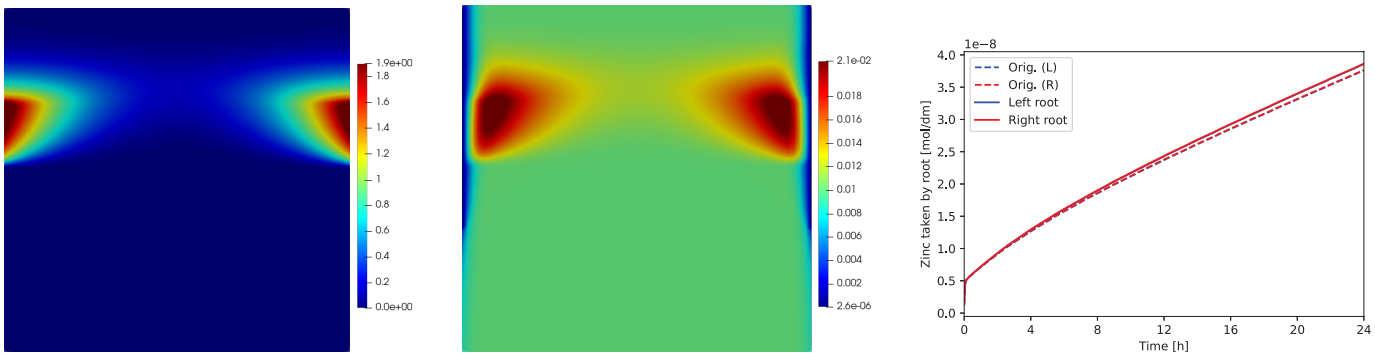

(a) DMA (b) Zn (c) Cumulative Zn uptake by the left (L) and right (R) root

Figure 11: DMA exudation rate F_Y increased by 10^{-11} and distance increased to $w = 0.15$ dm. In (a) concentration of DMA and (b) concentration of Zn after 24 hours in µM; (c) comparison of the amount of Zn absorbed by each root at distance $w = 0.15$ dm with original and increased exudation rate.

3.4.5 Increased Zn absorption power

If instead we increase the power of Zn absorption by the rice plant α, we see that the concentration plots in Figure 12a and 12b remain very similar compared to the benchmark result, although we see increase in Zn uptake in Figure 12c. Thus, in the case of allowing a plant to better utilise the Zn around it, this model suggests that when it comes to breeding rice plants it is better to focus on increasing the expression of genes geared towards DMA exudation than to increase transporter strength which would mirror the simulated increase in maximum Zn uptake here. Increased DMA exudation rate by just 1×10^{-11} mol dm^2 s^{-1} has a much larger impact upon Zn uptake than the larger increase of 5×10^{-3} mol plotted here giving an observably larger increase in Zn transported. Numerically, at the final 24 hours time in Figure 12c the root has a cumulative intake of 6.99×10^8 with the original parameters, while with the increased Zn absorption the uptake increases to 7.176×10^8, an increase of 2.661%.

4 Extended model

We will consider a model where two plants secrete two different exudates that act on a nutrient in the soil which is then absorbed through their roots. We then follow the derivation for a model of one plant described in [6]. The main change lies in modelling the dynamics of an extra nutrient which results in additional terms in the equation for dynamics of X and a new equation for the dynamics of the second

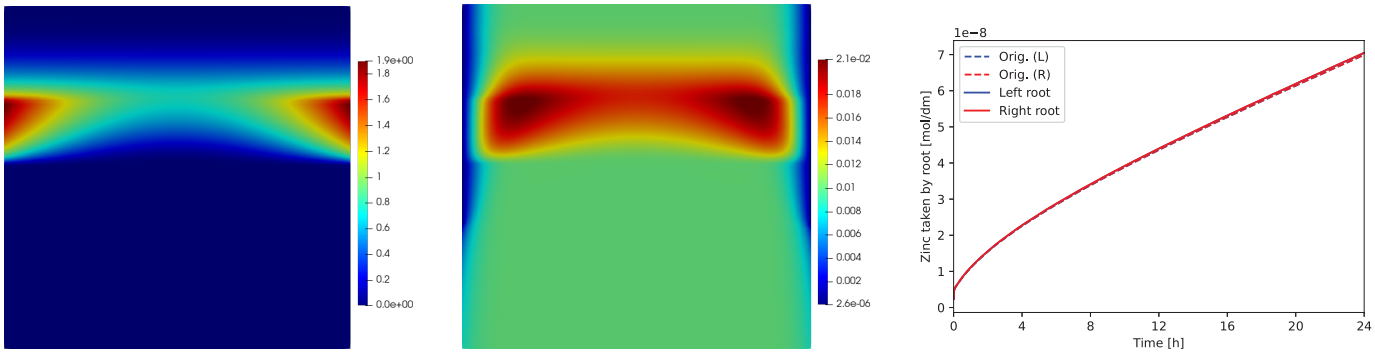

(a) DMA (b) Zn (c) Cumulative Zn uptake by the left (L) and right (R) root

Figure 12: Zn absorption power increased by 0.5×10^{-2}. In (a) concentration of DMA and (b) concentration of Zn after 24 hours in µM; (c) the amount of Zn absorbed by each root has slightly increased compared to the benchmark result.

exudate.

Our domain is a rectangle with a root one plant with certain features onthe left hand side and a second, different plant on the right hand side. Both exude some amount of each exudate Y_1, Y_2 however one may secrete more than the other. The concentrations of X, Y_1, and Y_2 in the soil solution will be marked by X_L, $Y_{L,1}$, and $Y_{L,2}$, while their concentrations in the soil solid in rapid equilibrium with the solution will be X_S, $Y_{S,1}$, and $Y_{S,2}$. The conservation equations for X, Y_1, and Y_2 in unit volume of soil are

$$\partial_t(\theta X_L + X_S) = \nabla \cdot (D_X \nabla X_L - \nu X_L) - g_X, \tag{4.1a}$$
$$\partial_t(\theta Y_{L,1} + Y_{S,1}) = \nabla \cdot (D_{Y,1} \nabla Y_{L,1} - \nu Y_{L,1}) - g_{Y,1}, \tag{4.1b}$$
$$\partial_t(\theta Y_{L,2} + Y_{S,2}) = \nabla \cdot (D_{Y,2} \nabla Y_{L,2} - \nu Y_{L,2}) - g_{Y,2}, \tag{4.1c}$$

with the involved parameters presented in Table 2. Next, we specify the equations for interaction between the nutrients in the solid and in the solution assuming Y_1 and Y_2 do not interact with each other. This is represented with the following system of ordinary differential equations

$$\partial X_S = \beta_1 X_L - \beta_2 X_S - \beta_3 X_S Y_{L,1} - \beta_4 X_S Y_{L,2}, \tag{4.2a}$$
$$\partial Y_{S,1} = \gamma_1 Y_{L,1} - \gamma_2 Y_{S,2} - \gamma_3 Y_{S,1} X_L, \tag{4.2b}$$
$$\partial Y_{S,2} = \xi_1 Y_{L,2} - \xi_2 Y_{S,2} - \xi_3 Y_{S,2} X_L, \tag{4.2c}$$

where β_1, β_2, β_3, β_4, γ_1, γ_2, γ_3, ξ_1, ξ_2, and ξ_3 are reaction rate coefficients. The existence of solutions of this coupled ODE-PDE system is studied in Section 7.

At equilibrium, equations (4.2) satisfy $\partial_t X_S = \partial_t Y_{S,1} = \partial_t Y_{S,2} = 0$, therefore

$$X_S = \frac{\beta_1 X_L}{\beta_2 + \beta_3 Y_{L,1} + \beta_4 Y_{L,2}}, \qquad Y_{S,1} = \frac{\gamma_1 Y_{L,1}}{\gamma_2 + \gamma_3 X_L}, \qquad Y_{S,2} = \frac{\xi_1 Y_{L,2}}{\xi_2 + \xi_3 X_L}. \tag{4.3}$$

We differentiate the terms in (4.3) with respect to time, which gives us

$$\partial_t X_S = \frac{\beta_1}{\beta_2 + \beta_3 Y_{L,1} + \beta_4 Y_{L,2}} \partial_t X_L - \frac{\beta_1 X_L \beta_3}{(\beta_2 + \beta_3 Y_{L,1} + \beta_4 Y_{L,2})^2} \partial_t Y_{L,1} - \frac{\beta_1 X_L \beta_4}{(\beta_2 + \beta_3 Y_{L,1} + \beta_4 Y_{L,2})^2} \partial_t Y_{L,2}, \tag{4.4a}$$
$$\partial_t Y_{S,1} = \frac{\gamma_1}{\gamma_2 + \gamma_3 X_L} \partial_t Y_{L,1} - \frac{\gamma_1 Y_{L,1} \gamma_3}{(\gamma_2 + \gamma_3 X_L)^2} \partial_t X_L, \qquad \partial_t Y_{S,2} = \frac{\xi_1}{\xi_2 + \xi_3 X_L} \partial_t Y_{L,2} - \frac{\xi_1 Y_{L,2} \xi_3}{(\xi_2 + \xi_3 X_L)^2} \partial_t X_L. \tag{4.4b}$$

Combining equations (4.1) and (4.4) yields

$$\left(\theta + \frac{\beta_1}{\beta_2 + \beta_3 Y_{L,1} + \beta_4 Y_{L,2}}\right)\partial_t X_L - \frac{\beta_1 X_L \beta_3}{(\beta_2 + \beta_3 Y_{L,1} + \beta_4 Y_{L,2})^2}\partial_t Y_{L,1} - \frac{\beta_1 X_L \beta_4}{(\beta_2 + \beta_3 Y_{L,1} + \beta_4 Y_{L,2})^2}\partial_t Y_{L,2} = \nabla \cdot (D_X \nabla X_L - \nu X_L) - g_X, \tag{4.5a}$$

$$\left(\theta + \frac{\gamma_1}{\gamma_2 + \gamma_3 X_L}\right)\partial_t Y_{L,1} - \frac{\gamma_1 Y_{L,1}\gamma_3}{(\gamma_2 + \gamma_3 X_L)^2}\partial_t X_L) = \nabla \cdot (D_{Y,1} \nabla Y_{L,1} - \nu Y_{L,1}) - g_{Y,1}, \tag{4.5b}$$

$$\left(\theta + \frac{\xi_1}{\xi_2 + \xi_3 X_L}\right)\partial_t Y_{L,2} - \frac{\xi_1 Y_{L,2}\xi_3}{(\xi_2 + \xi_3 X_L)^2}\partial_t X_L = \nabla \cdot (D_{Y,2} \nabla Y_{L,2} - \nu Y_{L,2}) - g_{Y,2}. \tag{4.5c}$$

The set of equations above can then be modified by dividing the numerator and denominator of each fraction by an adequate parameter. This way we obtain the final set of conservation equations in terms of X_L, $Y_{L,1}$, and $Y_{L,2}$:

$$\left(\theta + \frac{b_X}{1 + \kappa_{X,1} b_X Y_{L,1} + \kappa_{X,2} b_X Y_{L,2}}\right)\partial_t X_L - \frac{\kappa_{X,1} b_X^2 X_L}{\left(1 + \kappa_{X,1} b_X Y_{L,1} + \kappa_{X,2} b_X Y_{L,2}\right)^2}\partial_t Y_{L,1} - \frac{\kappa_{X,2} b_X^2 X_L}{\left(1 + \kappa_{X,1} b_X Y_{L,1} + \kappa_{X,2} b_X Y_{L,2}\right)^2}\partial_t Y_{L,2} = \nabla \cdot (D_X \nabla X_L - \nu X_L) - g_X, \tag{4.6a}$$

$$\left(\theta + \frac{b_{Y,1}}{1 + \kappa_{Y,1} b_{Y,1} X_L}\right)\partial_t Y_{L,1} - \frac{b_{Y,1}^2 \kappa_{Y,1} Y_{L,1}}{\left(1 + \kappa_{Y,1} b_{Y,1} X_L\right)^2}\partial_t X_L = \nabla \cdot (D_{Y,1} \nabla Y_{L,1} - \nu Y_{L,1}) - g_{Y,1}, \tag{4.6b}$$

$$\left(\theta + \frac{b_{Y,2}}{1 + \kappa_{Y,2} b_{Y,2} X_L}\right)\partial_t Y_{L,2} - \frac{b_{Y,2}^2 \kappa_{Y,2} Y_{L,2}}{\left(1 + \kappa_{Y,2} b_{Y,2} X_L\right)^2}\partial_t X_L = \nabla \cdot (D_{Y,2} \nabla Y_{L,2} - \nu Y_{L,2}) - g_{Y,2}, \tag{4.6c}$$

where $b_X = \beta_1/\beta_2$, $b_{Y,1} = \gamma_1/\gamma_2$, $b_{Y,2} = \xi_1/\xi_2$, $\kappa_{X,1} = \beta_3/\beta_1$, $\kappa_{X,2} = \beta_4/\beta_1$, $\kappa_{Y,1} = \gamma_3/\gamma_1$, $\kappa_{Y,1} = \xi_3/\xi_1$ are parameters presented in Table 2.

Finally, we will consider a simplification of the system of equations (4.6) in a regime where $\kappa_{Y,1} = \kappa_{Y,2} = 0$, i.e., the exudates do not interact with the metal. In this scenario we get the reduced system

$$\left(\theta + \frac{b_X}{1 + \kappa_{X,1} b_X Y_{L,1} + \kappa_{X,2} b_X Y_{L,2}}\right)\partial_t X_L - \frac{\kappa_{X,1} b_X^2 X_L}{\left(1 + \kappa_{X,1} b_X Y_{L,1} + \kappa_{X,2} b_X Y_{L,2}\right)^2}\partial_t Y_{L,1} - \frac{\kappa_{X,2} b_X^2 X_L}{\left(1 + \kappa_{X,1} b_X Y_{L,1} + \kappa_{X,2} b_X Y_{L,2}\right)^2}\partial_t Y_{L,2} = \nabla \cdot (D_X \nabla X_L - \nu X_L) - g_X, \tag{4.7a}$$

$$(\theta + b_{Y,1})\partial_t Y_{L,1} = \nabla \cdot (D_{Y,1} \nabla Y_{L,1} - \nu Y_{L,1}) - g_{Y,1}, \tag{4.7b}$$

$$(\theta + b_{Y,2})\partial_t Y_{L,2} = \nabla \cdot (D_{Y,2} \nabla Y_{L,2} - \nu Y_{L,2}) - g_{Y,2}. \tag{4.7c}$$

Symbol	Meaning
$D_{L,X}$	Diffusion of micronutrient X in free solution
$D_{L,Y,1}$	Diffusion of exudate Y_1 in free solution
$D_{L,Y,2}$	Diffusion of the exudate Y_2 in free solution
g_X	Function for immobilisation of X
$g_{Y,1}$	Function for decomposition of Y_1
$g_{Y,2}$	Function for decomposition of Y_2
b_X	Buffer power of X
$b_{Y,1}$	Buffer power of Y_1
$b_{Y,2}$	Buffer power of Y_2
$\kappa_{X,1}$	X – Y_1 interaction coefficient
$\kappa_{X,2}$	X – Y_2 interaction coefficient
$\kappa_{Y,1}$	Y_1 – X interaction coefficient
$\kappa_{Y,2}$	Y_2 – X interaction coefficient
α_1	X-absorbing power of root of plant 1
α_2	X-absorbing power of root of plant 1
$F_{Y,1}$	Rate of Y_1 exudation from plant 1
$F_{Y,2}$	Rate of Y_2 exudation from plant 2
L_1	Length of root of plant 1 at certain time, increases at rate G_1
L_2	Length of root of plant 1 at certain time, increases at rate G_2
$\delta L_{X,1}$	Length of X uptake zone at plant 1
$\delta L_{Y,1,1}$	Length of Y_1 secretion zone at plant 1
$\delta L_{X,2}$	Length of X uptake zone at plant 2
$\delta L_{Y,2,2}$	Length of Y_2 secretion zone at plant 2
a	Root radius of plant 1
w	Distance between the roots

Table 2: Table of parameters and their meanings for the extended model.

4.1 One exudate per root

The following boundary conditions are expanded upon the right-hand side boundary using the conditions from the base model and symmetry of the domain. On the left-hand side of the domain (plant 1) we have

$$D_X \partial_r X_L - \nu X_L = \alpha_1 X_L \qquad r = a, \quad z \in [-L_1, -(L_1 - \delta L_{X,1})], \tag{4.8a}$$
$$D_{Y_1} \partial_r Y_{L,1} - \nu Y_{L,1} = -F_{Y,1}(t) \qquad r = a, \quad z \in [-L_1, -(L_1 - \delta L_{Y,1,1})], \tag{4.8b}$$

and on the right-hand side of the domain (plant 2) we have

$$D_X \partial_r X_L - \nu X_L = -\alpha_2 X_L \qquad r = w + a, \quad z \in [-L_2, -(L_2 - \delta L_{X,2})], \tag{4.8c}$$
$$D_{Y_2} \partial_r Y_{L,2} - \nu Y_{L,2} = F_{Y,2}(t) \qquad r = w + a, \quad z \in [-L_2, -(L_2 - \delta L_{Y,2,2})]. \tag{4.8d}$$

Again, we consider zero-flux conditions for the rest of the boundary.

4.2 Two exudates at each root

We can further extend the model defined in this section so that both plants exude the same two exudates. This change is reflected only in the boundary conditions. On the left-hand side of the domain (plant 1) we add the exudation of Y_2,

$$D_X \partial_r X_L - \nu X_L = \alpha_1 X_L \qquad r = a, \quad z \in [-L_1, -(L_1 - \delta L_{X,1})] \tag{4.9a}$$
$$D_{Y_1} \partial_r Y_{L,1} - \nu Y_{L,1} = -F_{Y,1,1}(t) \qquad r = a, \quad z \in [-L_1, -(L_1 - \delta L_{Y,1,1})] \tag{4.9b}$$
$$D_{Y_2} \partial_r Y_{L,2} - \nu Y_{L,2} = -F_{Y,2,1}(t) \qquad r = a, \quad z \in [-L_1, -(L_1 - \delta L_{Y,2,1})] \tag{4.9c}$$

and on the right-hand side of the domain (plant 2) we add the exudation of Y_1,

$$D_X \partial_r X_L - \nu X_L = -\alpha_2 X_L \qquad r = w + a, \quad z \in [-L_2, -(L_2 - \delta L_{X,2})], \tag{4.9d}$$

$$D_{Y_1} \partial_r Y_{L,1} - \nu Y_{L,1} = F_{Y,1,2}(t) \qquad r = w + a, \quad z \in [-L_2, -(L_2 - \delta L_{Y,1,2})], \tag{4.9e}$$

$$D_{Y_2} \partial_r Y_{L,2} - \nu Y_{L,2} = F_{Y,2,2}(t) \qquad r = w + a, \quad z \in [-L_2, -(L_2 - \delta L_{Y,2,2})]. \tag{4.9f}$$

For our simulations we assume that both exudates at both plants are secreted 2cm behind the root tip. The exudation rates, secretion zone parameters and functions for decomposition and immobilisation are explained in Table 3, while the situation in the domain is shown in Figure 13.

Symbol	Meaning
$\delta L_{Y,1,1}$	Length of Y_1 secretion zone at plant 1
$\delta L_{Y,2,1}$	Length of Y_2 secretion zone at plant 1
$\delta L_{Y,1,2}$	Length of Y_1 secretion zone at plant 2
$\delta L_{Y,2,2}$	Length of Y_2 secretion zone at plant 2
$F_{Y,1,1}$	Rate of Y_1 exudation from plant 1
$F_{Y,2,1}$	Rate of Y_2 exudation from plant 1
$F_{Y,1,2}$	Rate of Y_1 exudation from plant 2
$F_{Y,2,2}$	Rate of Y_2 exudation from plant 2

Table 3: Additional parameters emerging from the boundary conditions when each root secretes both exudates.

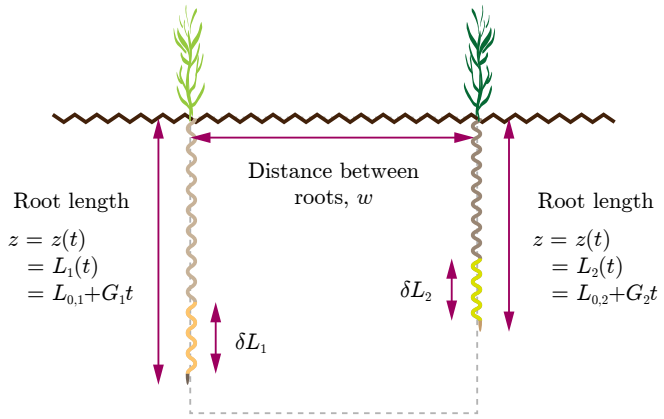

Figure 13: Sketch of the domain for system with two plants secreting two exudates.

4.3 Numerical approximation scheme

In this section we will outline the approximation scheme used to obtain numerical solutions of the extended model. The methods used follow the same lines of Section 3.3.

An scaling procedure similar to the one carried out in Section 3.3.1 is presented in Appendix C. There we identify the variables $\hat{x}$, $\hat{y}_1$, and $\hat{y}_2$ as the non-dimensionalised versions of X_L, $Y_{L,1}$, and $Y_{L,2}$, respectively. In what follows, we will use the non-dimensionalised quantities but will drop the *hat* decorator for brevity of presentation.

In this context, define the squared domain $\Omega = [0,1] \times [0,-1]$ and its boundary $\Gamma = \partial\Omega$. For each moment of time $t \in [0,1]$, we define the functions

$$A(y_1, y_2) := \theta + \frac{b_x}{1 + \kappa_{x,1} b_x y_1 + \kappa_{x,2} b_x y_2}, \qquad B(x, y_1, y_2) := \frac{\kappa_{x,1} b_x^2 x}{(1 + \kappa_{x,1} b_x y_1 + \kappa_{x,2} b_x y_2)^2},$$

and

$$C(x, y_1, y_2) := \frac{\kappa_{x,2} b_x^2 x}{(1 + \kappa_{x,1} b_x y_1 + \kappa_{x,2} b_x y_2)^2}.$$

Again we include a simple backward difference scheme with decoupling for finding solutions of (4.7) with boundary conditions (4.8) or (4.9). As before, we will discretise the time domain by $N + 1$ uniform steps of length Δt. The superscript n denotes a quantity at time t_n, where n is an integer counting time levels; e.g. x^n is x evaluated at the nth time point.

For the model on one exudate per root (4.8), we proceed to decouple the parabolic system of differential equations by linearising its nonlinear terms using previous updates. Here we observe that the parabolic systems on y_1 and y_2 are simpler to solve, as they do not depend explicitly on x. The resulting scheme is as follows. Initialising $\hat{x}^0 = \hat{x}_0$ and $\hat{y}^0 = \hat{y}_0$, then for every $n \in \{0, \dots, N\}$: (A) Solve the variational problem of finding y_1^{n+1} such that

$$\int_\Omega (\theta + b_{y,1})(y_1^{n+1} - y_1^n) v \,\mathrm{d}\mu = \Delta t \int_{\Gamma_{1,y}^{n+1}} F_{y,1}^n v \,\mathrm{d}\sigma - \Delta t \int_\Omega (D_{y,1} \nabla y_1^{n+1} - \nu y_1^{n+1}) \cdot \nabla v \,\mathrm{d}\mu - \Delta t \int_\Omega g_{y,1}^n v \,\mathrm{d}\mu, \quad (4.10a)$$

for every $v \in H^1(\Omega)$. (B) Also find y_2^{n+1} that solves

$$\int_\Omega (\theta + b_{y,2})(y_2^{n+1} - y_2^n) v \,\mathrm{d}\mu = \Delta t \int_{\Gamma_{2,y}^{n+1}} F_{y,2}^n v \,\mathrm{d}\sigma - \Delta t \int_\Omega (D_{y,2} \nabla y_2^{n+1} - \nu y_2^{n+1}) \cdot \nabla v \,\mathrm{d}\mu - \Delta t \int_\Omega g_{y,2}^n v \,\mathrm{d}\mu, \quad (4.10b)$$

for every $v \in H^1(\Omega)$. (C) Proceed on finding x^{n+1} such that it satisfies

$$\begin{aligned} &\int_\Omega A(y_1^n, y_2^n)(x^{n+1} - x^n) v - B(x^n, y_1^n, y_2^n)(y_1^{n+1} - y_1^n) v - C(x^n, y_1^n, y_2^n)(y_2^{n+1} - y_2^n) v \,\mathrm{d}\mu \\ &\quad = -\Delta t \int_{\Gamma_{2,x}^{n+1}} \alpha_2 x^{n+1} v \,\mathrm{d}\sigma - \Delta t \int_{\Gamma_{1,x}^{n+1}} \alpha_1 x^{n+1} v \,\mathrm{d}\sigma - \Delta t \int_\Omega (D_x \nabla x^{n+1} - \nu x^{n+1}) \cdot \nabla v \,\mathrm{d}\mu - \Delta t \int_\Omega g_x^n v \,\mathrm{d}\mu, \end{aligned} \quad (4.10c)$$

for every $v \in H^1(\Omega)$.

The segments $\Gamma_{1,y}^{n+1}$, $\Gamma_{2,y}^{n+1}$, $\Gamma_{1,x}^{n+1}$, and $\Gamma_{2,x}^{n+1}$ are updated at each time level t_{n+1}. They are implicitly defined by the boundary conditions (4.8).

In the case of two exudates the numerical approach is similar. The only differences are that the surface integral in (4.10a) is replaced with $\Delta t \Big(\int_{\Gamma_{1,1,y}^{n+1}} F_{y,1,1}^n v \,\mathrm{d}\sigma + \int_{\Gamma_{1,2,y}^{n+1}} F_{y,1,2}^n v \,\mathrm{d}\sigma \Big)$; and likewise the surface term in (4.10b) is replaced with $\Delta t \Big(\int_{\Gamma_{2,1,y}^{n+1}} F_{y,2,1}^n v \,\mathrm{d}\sigma + \int_{\Gamma_{2,2,y}^{n+1}} F_{y,2,2}^n v \,\mathrm{d}\sigma \Big)$. Here the sub subsets of Γ are defined implicitly by conditions (4.9).

5 Results of the extended model

In this section, we use the system (4.7) with boundary conditions (4.9) to model a system with barley and tobacco plant combination. First, we clarify the choice of parameters used for the system, and then we present and analyse the simulation results.

5.1 Parameters for barley-tobacco combination

In the following subsections we discuss the selection of parameters in Table 4 to model the dynamics between exudates of barley and tobacco plants and P in the soil.

Symbol	Meaning	Value
θ	Solution volume fraction	$0.2 - 0.3\ \mathrm{dm^3\,dm^{-3}}$
f	Diffusion impedance factor	0.5
ρ	Soil bulk density	$1.2\ \mathrm{kg\,dm^{-3}}$
$D_{L,X}$	Diffusion coefficient of phosphate in free solution	$7 - 9 \times 10^{-8}\ \mathrm{dm^2\,s^{-1}}$
$D_{L,Y,1}$	Diffusion of phytase in free solution	$3.5 - 4.5 \times 10^{-8}\ \mathrm{dm^2\ s^{-1}}$
$D_{L,Y,2}$	Diffusion of citrate in free solution	$2.1 \times 10^{-8}\ \mathrm{dm^2\,s^{-1}}$
ν	Water flux	$1 \times 10^{-6}\ \mathrm{dm\,s^{-1}}$
g_X	Function for phosphate immobilisation	0
$g_{Y,1}$	Function for phytase decomposition	0
$g_{Y,2}$	Function for citrate decomposition	$\frac{\rho V_{\max} Y_{L,2}}{K_M + Y_{L,2}}$ where $V_{\max} = 0$ or $V_{\max} = 2.5 \times 10^{-9}\ \mathrm{mol\,kg^{-1}\,s^{-1}}$, $K_M = 10^{-8}$ M
b_X	Phosphate buffer power	300 – 2200
$b_{Y,1}$	Phytase buffer power	1
$b_{Y,2}$	Citrate buffer power	1
$\kappa_{X,1}$	Phosphate - phytase interaction coefficient	$18.43\ \mathrm{dm^3\,mol^{-1}}$
$\kappa_{X,2}$	Phosphate - citrate interaction coefficient	$92.16\ \mathrm{dm^3\,mol^{-1}}$
$\kappa_{Y,1}$	Phytase - phosphate interaction coefficient	0
$\kappa_{Y,2}$	Citrate - phosphate interaction coefficient	0
α_1	Phosphate absorbing power of root of barley	$5.6 \times 10^{-3}\ \mathrm{dm\,s^{-1}}$
α_2	Phosphate absorbing power of root of tobacco	$5.6 \times 10^{-3}\ \mathrm{dm\,s^{-1}}$
$F_{Y,1,1}$	Rate of phytase exudation in barley	$2.466 \times 10^{-11} - 2.503 \times 10^{-10}\ \mathrm{mol\,dm^{-2}\,s^{-1}}$
$F_{Y,2,1}$	Rate of citrate exudation in barley	$1.097 \times 10^{-12} - 1.006 \times 10^{-9}\ \mathrm{mol\,dm^{-2}\,s^{-1}}$
$F_{Y,1,2}$	Rate of phytase exudation in tobacco	$1.316 \times 10^{-6}\ \mathrm{mol\,dm^{-2}\,s^{-1}}$
$F_{Y,2,2}$	Rate of citrate exudation in tobacco	$2.722 \times 10^{-6}\ \mathrm{mol\,dm^{-2}\,s^{-1}}$
L_1	Barley root length	increases at rate $G_1 = 0.1728\ \mathrm{dm\,day^{-1}}$
L_2	Tobacco root length	increases at rate $G_2 = 0.2\ \mathrm{dm\,day^{-1}}$
$\delta L_{X,1}$	Length of phosphate uptake zone at barley	L_1
$\delta L_{Y,1,1}$	Length of phytase secretion zone at barley	0.2 dm
$\delta L_{Y,1,2}$	Length of citrate secretion zone at barley	0.2 dm
$\delta L_{X,2}$	Length of phosphate uptake zone at tobacco	L_2
$\delta L_{Y,1,2}$	Length of phytase secretion zone at tobacco	0.2 dm
$\delta L_{Y,2,2}$	Length of citrate secretion zone at tobacco	0.2 dm
a	Root radius of barley	0.005 dm
w	Distance between the roots	varied

Table 4: Table of parameters with their meanings and values used for numerical experiments in this section, plant 1 (LHS) is barley, plant 2 (RHS) is tobacco, component X is phosphate, Y_1 is phytase, and Y_2 is citrate.

5.1.1 Soil parameters

We choose the water content in soil θ to be in the range 0.2 to 0.3 which should be in accordance with real- life conditions in which tobacco and barley are cultivated [19], along with estimated soil bulk density $\rho = 1.2\ \mathrm{kgdm^{-3}}$. We keep the impedance factor the same as in [6], i.e. $f = 0.5$.

5.1.2 Diffusion coefficients

We take the range of phosphate diffusion in water from [20] where $D_{L,X} = 9 \times 10^{-8}\ \mathrm{dm^2\,s^{-1}}$ and from [13] where $D_{L,X} = 7 \times 10^{-8}\ \mathrm{dm^2\,s^{-1}}$. In [13] we also have citrate diffusion in free solution $D_{L,Y,2} = 2.1 \times 10^{-8}\ \mathrm{dm^2\,s^{-1}}$. We estimate phytase diffusion to be half of phosphate diffusion, i.e. $D_{L,Y,1}$ in the range $3.5 - 4.5 \times$

10^{-8} dm^2 s^{-1}, as its molecules are bigger so it will diffuse more slowly [19]. Diffusion of the micronutrients in soil is calculated as $D_X = D_{L,X} f\theta$, $D_{Y,1} = D_{L,Y,1} f\theta$, and $D_{Y,2} = D_{L,Y,2} f\theta$. In the table we also state the value for water flux coefficient ν, however, following the findings in [6] we consider $\nu = 0$.

5.1.3 Parameters for sorption, mutual interaction, and decomposition

From the derivation of the extended model we recall that the phosphate buffer power is $b_X = \beta_1/\beta_2$, where β_1, β_2 are parameters for adsorption and desorption to and from soil particles, respectively. The typical range for b_X is taken from [20]. For further derivation we take β_1, β_2 from [20] where $\beta_1 = 3.7 \times 10^{-6}$ s^{-1}, $\beta_2 = 4.68 \times 10^{-9}$ s^{-1}. For simplicity we assume $b_{Y,1} = b_{Y,2} = 1$. The parameter for $X - Y_2$ interaction is $\kappa_{X,2} = \beta_4/\beta_1$ where β_4 is phosphate enhanced desorption from soil solid due to absorbed citrate. The value $\beta_4 = 3.41 \times 10^{-4}$ is from [13], and it gives us $\kappa_{X,2} = 92.16$ dm^3 mol^{-1}. We estimate the coefficient for $X - Y_1$ interaction, $\kappa_{X,1}$, to be 5-fold smaller than $\kappa_{X,2}$ [19]. Furthermore, we consider the parameters for interaction of the exudates with phosphate ($\kappa_{Y,1}$ and $\kappa_{Y,2}$) to be zero.

Similarly to [6], we assume that there are no reactions in the soil that involve decomposition of phosphate, i.e. $g_X = 0$. For the decomposition of citrate we might consider a Michaelis-Menten-type term $g_{Y,2} = V_{\max} Y_{L,2}/(K_M + Y_{L,2})$, however, sorption of citrate to soil particles causes up to 99% reduction in biodegradation rate [13]. We therefore choose $V_{\max} = 0$ and experiment with non-zero values similar to those in [6]. For phytase we also set $g_{Y,1} = 0$ since we assume no microbial consumption of this nutrient [19].

5.1.4 Absorption power and exudation rates

The coefficients for exudation rates in barley are taken from [21]. Tobacco exudation rates were obtained from [14] where we tried to estimate the root surface by using root radius being half of barley root radius (i.e. $a_2 = 2.5 \times 10^{-3}$) and the length of the root 100 dm, approximating the root(s) as a cylinder [19]. However, this way both $F_{Y,1,2}$ and $F_{Y,2,2}$ were of order 10^{-6} which is much larger than the order of magnitude of $F_{Y,1,1}$ and $F_{Y,2,1}$ being 10^{-10}. These relatively large exudation rates caused issues in the numerical simulations. We therefore didn't use the computed values $F_{Y,1,2}$ and $F_{Y,2,2}$ as described above, but we multiplied them by 10^{-4} so that all the exudation rates are of order 10^{-10}. This may cause some inaccuracy in our simulations however it is necessary due to the lack of data on this subject.

5.1.5 Geometry of the domain

The domain's main axes are r (horizontal) and z (vertical), see Figure 13. For the simulations we chose the distance between the two roots (i.e. the width of the simulation window) to be $w = 0.04$ dm. The height of the simulation window is chosen to be the length of one of the roots after 3-day growth. In both plants, phosphate is absorbed along the whole length of root. For the exudation we choose to locate the 2 cm long exudation zone to be 2 cm behind the root tip (i.e. before the root cap), see Figure 3.

5.2 Numerical experiments

In this section, we will numerically solve the non-dimensionalised version of model (4.7) with boundary conditions (4.9) using FEniCS. To find out the effects of changes in parameters on phosphate uptake, we will take the set of parameter values in Table 6 as "original parameters" to get benchmark results. We then vary some of these parameters and describe the differences in the uptake. The total simulation time we choose is 24 hours, with time-step size $\Delta t = 0.01$. The FEniCS code is available in the repository mentioned in Appendix A. We must note that in the numerical experiments we have encountered negative values in the concentration plots which is not biologically feasible, we consider this an area for potential improvement

in the future. However, this error should not have much impact on the overall dynamics of the exudates with phosphate.

5.2.1 Benchmark result

For the first simulation we choose the set of parameters presented in Table 6 (see Appendix B) and plot the concentrations of phosphate, phytase, and citrate in soil solution after 24 hours, see Figure 14. We can clearly see that the root on the LHS has stronger exudation of phytase, while the root on the RHS has more prominent secretion of citrate, which is in accordance with the exudation rates we used. When comparing the two exudates we can also see that the effect of diffusion is more visible in phytase as the exudate gets transported into the middle of the domain, further away from the roots. The importance of diffusion coefficient will be therefore further investigated in the next subsections, along with the effect of exudation rate and uptake power of the roots. Another important feature is the buffer power of phosphate, i.e. the ratio of absorption and desorption to and from soil particles. We can hypothesise that with increased buffer power (which can be interpreted as increased absorption or decreased desorption rate), the nutrients will be absorbed to soil particles more quickly which will have a negative impact on phosphate uptake. Also, as mentioned previously, we will experiment with the effect of microbial consumption of citrate, predicting that it will have only a minor effect on the uptake of phosphate.

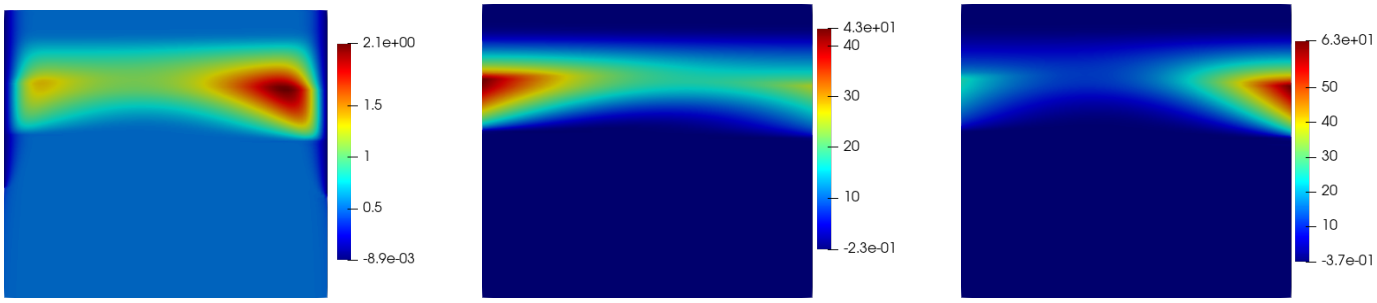

(a) Phosphate (X) (b) Phytase (Y_1) (c) Citrate (Y_2)

Figure 14: Concentrations of the nutrients in the soil solution between the two roots after 24 hours, in µM.

5.2.2 Citrate consumption by microbes

The first parameter change we experiment with is the assumption that citrate gets consumed by microbes in the soil, which we achieve by setting $V_{\max} = 2.5 \times 10^{-9}\ \mathrm{mol\,kg^{-1}\,s^{-1}}$ in the term for Y_2 decomposition $g_{Y,2} = \rho V_{\max} Y_{L,2}/(K_M + Y_{L,2})$. Comparing the values in the colourbar of Figure 15a with Figure 14a we see that the maximum concentration of phosphate in the soil solution decreased by $\sim$ 30%. More important information on how much phosphate was actually absorbed by the root is shown in Figure 15c where we can see curves showing cumulative uptake in comparison with the benchmark result. The difference in phosphate uptake caused by citrate microbial consumption is shown in Table 5, reaching -2.9% and -5.08% in the left and right root, respectively. The amount of drop in phosphate absorption depends mainly on the uptake power of each of the roots (which are the same in this set-up) and on the citrate exudation rate of the corresponding root which is the reason why there was larger drop in the root on the right. The value of $V_{\max}$ and the form of the citrate decompositon function was taken from the Zn–DMA model in [6], therefore the real dynamics for the actual decomposition of citrate may differ slightly.

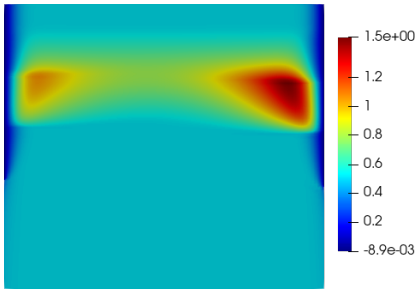

(a) Phosphate (X)

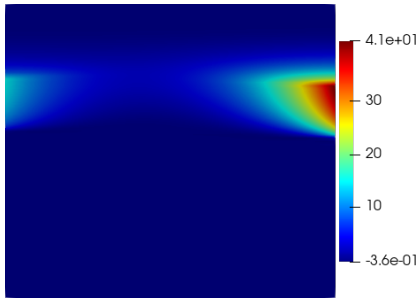

(b) Citrate (Y_2).

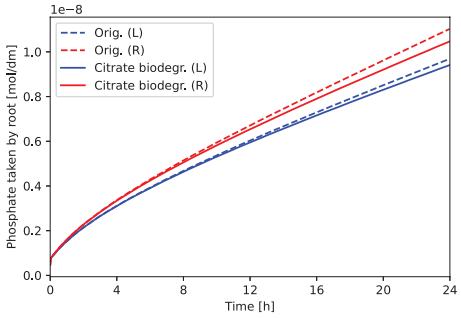

(c) Cumulative uptake of phosphate by the left (L) and right (R) root.

Figure 15: $V_{\max} = 2.5 \times 10^{-9}$ mol kg^{-1} s^{-1}, i.e. citrate gets consumed by microbes. In (a) concentration of phosphate and (b) citrate in soil solution between the two roots after 24 hours in µM; (c) comparison of phosphate absorbed by each of the roots with original (dashed line) and changed parameters (solid line).

5.2.3 Uptake power

We now explore what effect does tenfold increase or decrease in uptake power of the left root, α_1, have in comparison to the benchmark results. In Figures 16b and 16d we see the expected increase and decrease in phosphate uptake by the left root. In Table 5 we can observe that the tenfold raise in α_1 caused 22.6% more phosphate to be absorbed, while tenfold drop in the uptake power resulted in decline by only 6%. We can therefore assume that this root is more sensitive towards the increase in the uptake power. By comparing Figures 16a and 16c we do not notice a major difference in X_L besides a longer phosphate-deprived zone at the left edge of Figure 16a.

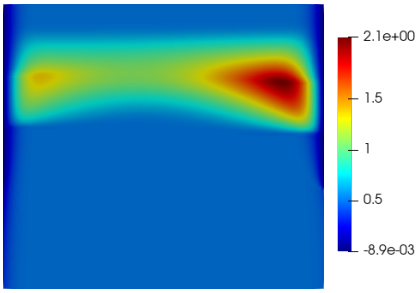

(a) Phosphate (X) with $\alpha \times 10$

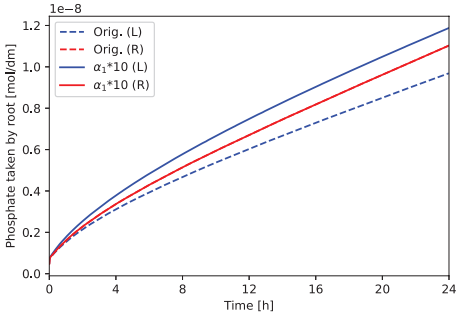

(b) Cumulative uptake of phosphate by the left (L) and right (R) root with $\alpha \times 10$.

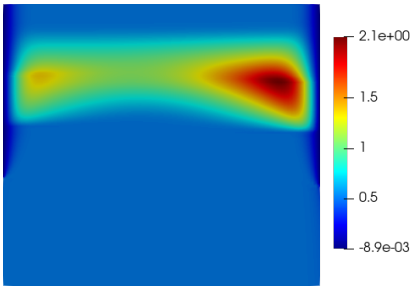

(c) Phosphate (X) with $\alpha/10$

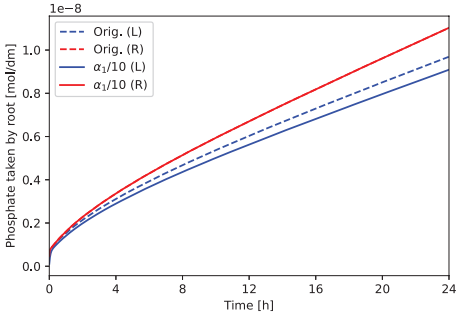

(d) Cumulative uptake of phosphate by the left (L) and right (R) root with $\alpha/10$.

Figure 16: Change in phosphate uptake power α_1. In (a) and (c) concentration of phosphate between the two roots after 24 hours in µM; (b) and (d) comparison of phosphate absorbed by each of the roots with original and changed parameters.

5.2.4 Phosphate buffer power

Next, we look at the buffer power b_X, which is defined as the ratio of absorption and desorption of phosphate to and from soil particles. First, we consider a twofold increase in b_X which can be thought of as $b_X \times 2 = \beta_1/(\beta_2/2)$, i.e. we reduce the desorption rate by a half. The implications of this change can be observed in Figure 17b. The results are somewhat counter-intuitive at first glance as we would expect that the decreased desorption rate (or equivalently, an increased absorption rate) would cause less phosphate to be absorbed by the root as it would stick to the soil particles instead of being released into the soil solution. We can also explain this intuitive thinking algebraically by taking (4.3) and expressing the ratio between phosphate concentration in soil solution and soil solid,

$$\frac{X_L}{X_S} = \frac{1}{b_X} + \kappa_{X,1} Y_{L,1} + \kappa_{X,2} Y_{L,2}, \tag{5.1}$$

we see that with increased b_X, the concentration of X in soil solid increases at the expense of X_L. However, we justify the actual results by supposing that the exudates operate on P at soil particles, i.e. they solubilise P they find at soil particles, and the more P is found there (the higher the buffer power), the more of it gets solubilised into the solution and transported to the root surface. Citrate, in particular, pushes organic phosphate from the soil particles into the soil solution where phytase acts on it. This observation is very interesting as we didn't model the process into such details, and can be explored further in future work.

We may consider the opposite of the previous scenario and divide b_X by two, i.e. $b_X/2 = \beta_1/(2\beta_2)$, so we increase the desorption rate from soil particles. We now expect that this will have the opposite effect to what we have observed in Figure 17b. In Figure 17d we can see a decrease in phosphate uptake by both roots. Besides the huge difference between the range of values in Figure 17a and 17c, we notice in Table 5 that decreased buffer power results in a greater absolute change in absorbed phosphate.

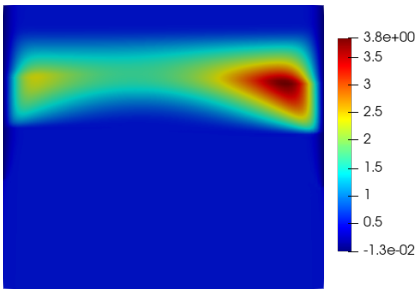

(a) Phosphate (X) with $b_X \times 2$

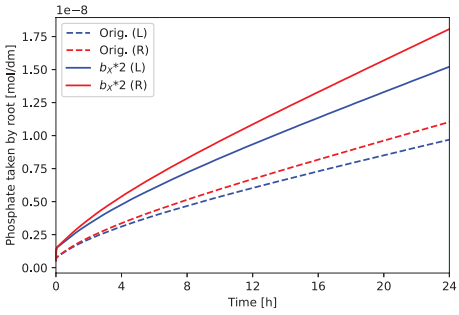

(b) Cumulative uptake of phosphate by the left (L) and right (R) root with $b_X \times 2$.

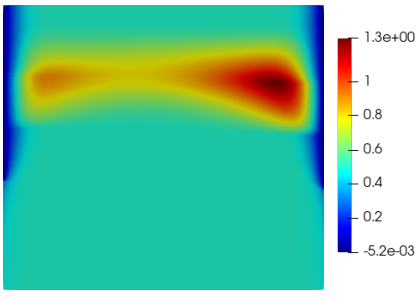

(c) Phosphate (X) with $b_X/2$

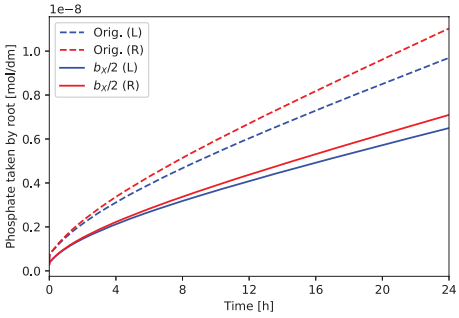

(d) Cumulative uptake of phosphate by the left (L) and right (R) root with $b_X/2$.

Figure 17: Change in buffer power b_X. In (a) and (c) concentration of phosphate between the two roots after 24 hours in µM; (b) and (d) comparison of phosphate absorbed by each of the roots with original and changed parameters.

5.2.5 Exudates buffer power

Now we examine the effect of change in buffer power of each of the exudates. Although we assumed $b_{Y,1} = b_{Y,2} = 1$, we can still try to play with these values to see what effect they have on phosphate uptake.

Previously we have seen that an increase in b_X resulted in more phosphate absorbed by the roots. While b_X was located in multiple non-linear terms in the system and its effect on the result was not clear at first sight, we can see that $b_{Y,1}$ and $b_{Y,2}$ are only present in the coefficient multiplying the time derivative of $Y_{L,1}$ and $Y_{L,2}$, respectively, since we took $k_{Y,1} = k_{Y,2} = 0$ for simplification. If we divide the equation by this coefficient, we see that a higher buffer power will cause smaller change in the exudate concentration throughout time. We therefore expect a decrease in phosphate uptake with increased $b_{Y,1}$ and $b_{Y,2}$, and vice versa. The numerical experiments support this hypothesis - in Figure 18b and 19b we can see that an increase in $b_{Y,1}$ and $b_{Y,2}$ resulted in less phosphate absorbed by the root, while the opposite trend can be seen in Figure 18d and 19d where we decreased these parameters.

Looking at the concentration plots of the exudates we notice that for higher buffer powers (Figures 18a and 19a) the chemicals didn't reach the middle of the domain, i.e. this change prohibited the exudates to get further away from the root. This resulted in less phosphate solubilised and absorbed by the roots, compared to the opposite scenario where the decrease of buffer powers enhanced the transport of the exudates in the rhizosphere (Figures 18c and 19c), which resulted in an increase in uptake by both roots. If we think of the buffer power again as a ratio between the absorption and desorption rate of the exudate, we can explain this effect by noticing that an increase in absorption rate (i.e. increase in buffer power) keeps the exudates more fixed to the soil particles which prohibits their diffusion in the rhizosphere.

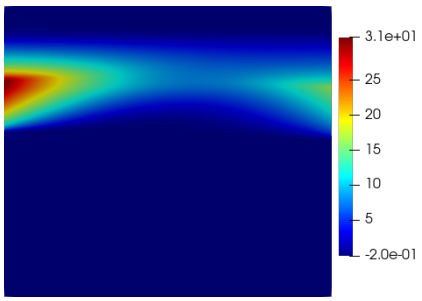

(a) Phytase (Y_1) with $b_{Y,1} \times 2$

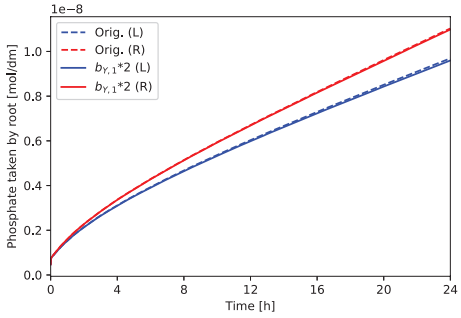

(b) Cumulative uptake of phosphate by the left (L) and right (R) root with $b_{Y,1} \times 2$.

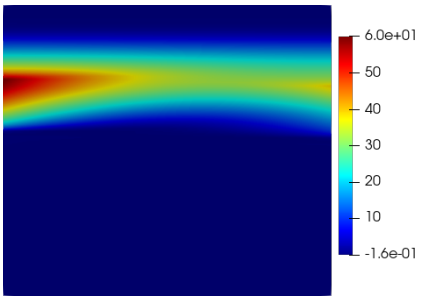

(c) Phytase (Y_1) with $b_{Y,1}/2$

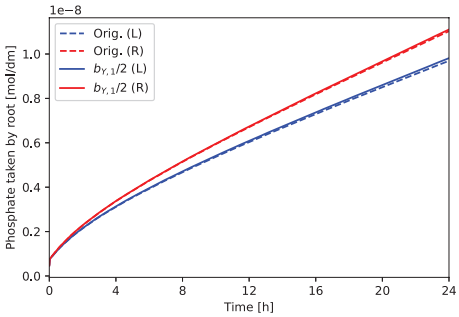

(d) Cumulative uptake of phosphate by the left (L) and right (R) root with $b_{Y,1}/2$.

Figure 18: Change in buffer power $b_{Y,1}$. In (a) and (c) concentration of phytase between the two roots after 24 hours in µM; (b) and (d) comparison of phosphate absorbed by each of the roots with original and changed parameters.

5.2.6 Diffusion coefficients

We can experiment with the effect of an increase of diffusion coefficients (in free solution) on the transport of the chemicals in the rhizosphere. We start with the diffusion coefficient of phosphate $D_{L,X}$ - in Figures

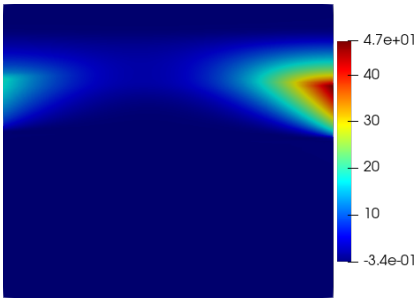

(a) Citrate (Y_2) with $b_{Y,2} \times 2$

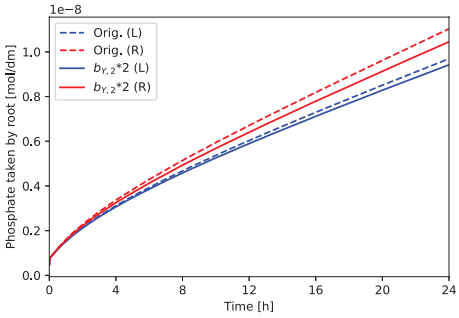

(b) Cumulative uptake of phosphate by the left (L) and right (R) root with $b_{Y,2} \times 2$.

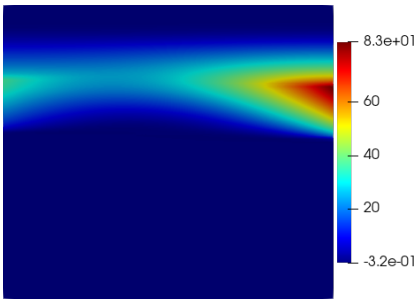

(c) Citrate (Y_2) with $b_{Y,2}/2$

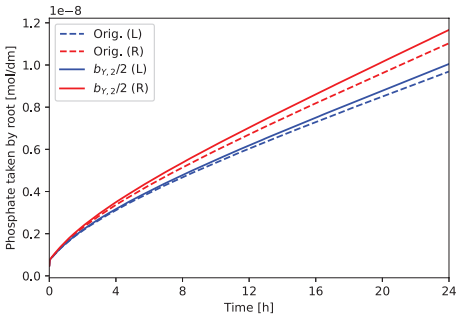

(d) Cumulative uptake of phosphate by the left (L) and right (R) root with $b_{Y,2}/2$.

Figure 19: Change in buffer power $b_{Y,2}$. In (a) and (c) concentration of citrate between the two roots after 24 hours in µM; (b) and (d) comparison of phosphate absorbed by each of the roots with original and changed parameters.

20b and Table 5 we see that increased phosphate diffusion had a positive effect on phosphate uptake. This might be explained by the exudates being secreted at the exudation zone of the root solubilising P and the following diffusion of phosphate into the surrounding area, making it accessible closer to the root. However, we do not see any visible change when comparing Figure 20a with the benchmark Figure 14a.

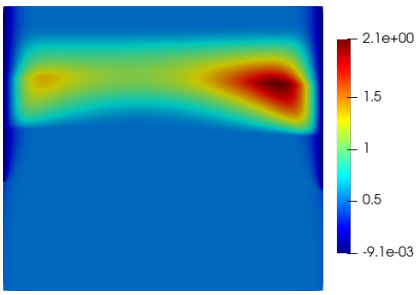

(a) Phosphate (X)

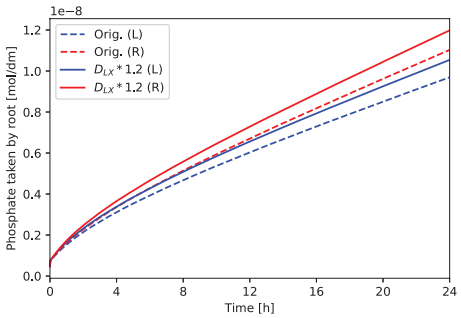

(b) Cumulative uptake of phosphate by the left (L) and right (R) root.

Figure 20: Phosphate diffusion coefficient $D_{L,X}$ increased by 20%. In (a) concentration of phosphate between the two roots after 24 hours in µM; (b) comparison of phosphate absorbed by each of the roots with original and changed parameters.

Similarly, we want to see what effect does increased diffusion of an exudate, e.g. $D_{L,Y,1}$, have on phosphate uptake. Although not visible in Figure 21b, in Table 5 we see a very small decrease in phosphate absorption. This can be explained by phytase being diffused further away from the root, therefore P is solubilised further away from the root and it takes it longer to reach its surface. By comparing the values in Figure 21a with 14b we see that with increased diffusion, the exudate doesn't reach concentrations as high as with the original parameter setup. We also experimented with increasing both $D_{L,Y,1}$ and $D_{L,Y,2}$ by 20% at the same time, which as expected resulted in a decrease in phosphate uptake. Although an increase in all three diffusion coefficients resulted in an overall increased phosphate uptake (+8.1% and +7.52%), this

value was lower than when considering only increased $D_{L,X}$ (+8.8% and +8.61%), see Table 5 for results of all numerical experiments.

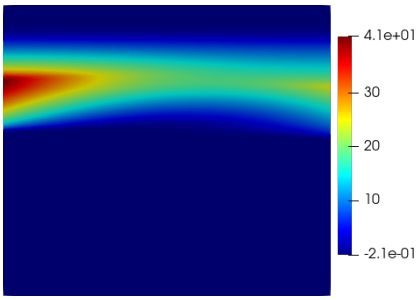

(a) Phytase (Y_1)

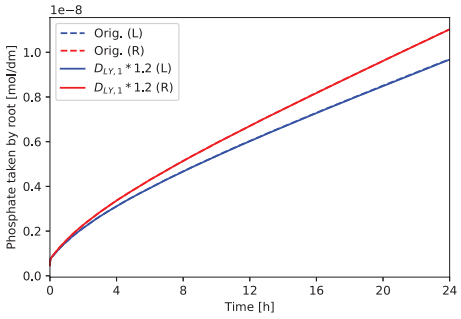

(b) Cumulative uptake of phosphate by the left (L) and right (R) root.

Figure 21: Phytase diffusion coefficient $D_{L,Y,1}$ increased by 20%. In (a) concentration of phosphate between the two roots after 24 hours in µM; (b) comparison of phosphate absorbed by each of the roots with original and changed parameters.

5.2.7 Phytase exudation rate

Possibly one of the most important factors that have effect on phosphate uptake is the rate at which the exudates are secreted from the roots as this is directly linked to solubilising P and therefore making more phosphate available for the root. We will experiment with changing exudation rate of phytase at the left root, i.e. $F_{Y,1,1}$, and combine it with changes in the diffusion coefficients.

First, we consider a 10-fold increase in phytase exudation rate at left root, i.e. $F_{Y,1,1}$. As one may have expected, this has an effect primarily on the root concerned, see Figure 22b. We also notice a 1% increase in uptake at the right root, see Table 5, which is one of the benefits of intercropping - a stronger exudation rate at one plant can help the neighbouring plant to absorb more nutrients. The amount by which the root on the left helps root on the right in this scenario might depend on more factors, for example the proximity of the roots (w), and the diffusion coefficient of the exudate.

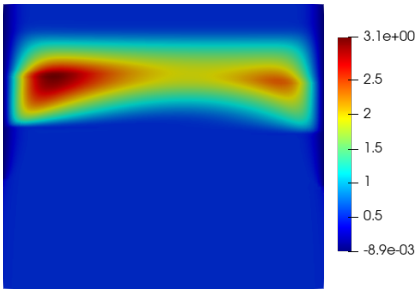

(a) Phosphate (X)

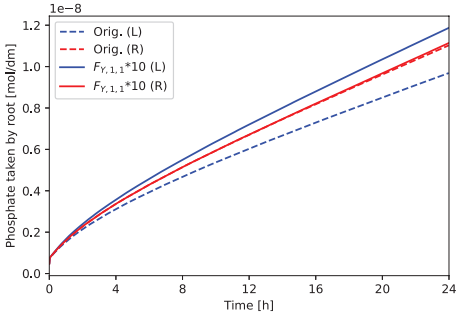

(b) Cumulative uptake of phosphate by the left (L) and right (R) root.

Figure 22: Phytase exudation rate power $F_{Y,1,1}$ multiplied by 10. In (a) concentration of phosphate between the two roots after 24 hours in µM; (b) comparison of phosphate absorbed by each of the roots with original and changed parameters.

Interestingly, in Table 5 we see that increasing diffusion of phytase by 20% really contributed positively towards phosphate uptake at the opposite root, while less nutrient was absorbed at the left root than without increasing diffusion. Thus, with increased diffusion and exudation at the left root, more phosphate gets absorbed at the right root at the price of less phosphate being absorbed at the left root.

In Figure 23 we see the effect of the distance between the roots before and after increasing $F_{Y,1,1}$. Shortening the distance between the roots by half resulted in $>$ 100% increase in phosphate uptake at both roots. Combining this with higher $F_{Y,1,1}$, we gain even more phosphate into each of the roots, this can be best seen

by comparing Figures 22b, 23b, and 23d and corresponding values in Table 5. We can see that with roots closer to each other and exudation rate increased, the root on the left actually gets more phosphate overall than the root on the right, which hasn't happened in any of the previous experiments.

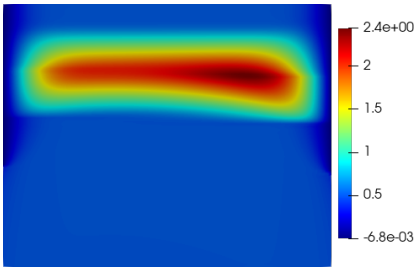

(a) Phosphate (X) with $w/2$

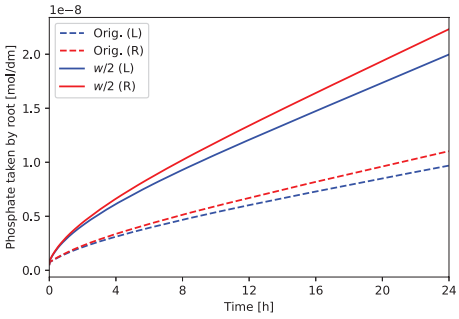

(b) Cumulative uptake of phosphate by the left (L) and right (R) root with $w/2$

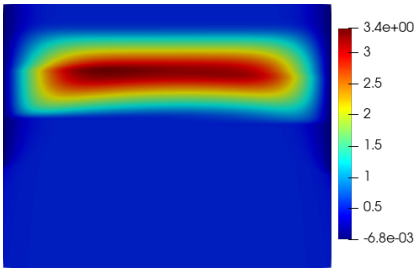

(c) Phosphate (X) with $w/2$ and $F_{Y,1,1} \times 10$

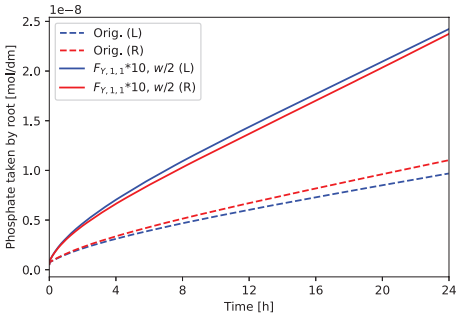

(d) Cumulative uptake of phosphate by the left (L) and right (R) root with $w/2$ and $F_{Y,1,1} \times 10$

Figure 23: Change in distance between the roots w and in phytase exudation rate power $F_{Y,1,1}$. In (a) and (c) concentration of phosphate between the two roots after 24 hours in µM; (b) and (d) comparison of phosphate absorbed by each of the roots with original and changed parameters.

5.2.8 Interaction coefficients

Since the role of the phosphate-phytase ($\kappa_{X,1}$) and phosphate-citrate ($\kappa_{X,2}$) interaction coefficients is not clear, we will vary their values to try to understand their role in the system. Since we have defined $\kappa_{X,1} = \kappa_{X,2}/5$, it is enough for us to change the value of $\kappa_{X,2}$ as this has effect on both parameters.

In Figures 24b and 24d we see that a 20% increase in interaction coefficients results in more phosphate absorbed, with the opposite effect resulting from decreasing the coefficients by 20%. Comparing the values of phosphate concentration in Figures 24a and 24c we notice that increased interaction enabled more phosphate to accumulate at certain place in the domain, while decreased interaction

The interaction coefficient $\kappa_{X,2}$ is mathematically defined as the ratio β_4/β_1, where β_4 is phosphate desorption from soil solid due to absorbed citrate, and β_1 is adsorption of phosphate to soil particles. Thus, by increasing $\kappa_{X,2}$ we also increase β_4 which results in citrate pushing more phosphate from soil solid into soil solution, therefore there is more phosphate available to be utilised by the root (as phytase has more P to solubilise in the soil liquid). We can apply similar reasoning to the coefficient $\kappa_{X,1}$, although the underlying biological explanation may be different.

6 Conclusions

In section 3.4 we experimented with the effect of the proximity of two identical roots secreting one exudate. We found that if the zones of root influence of the two roots do not intersect, very little interaction among

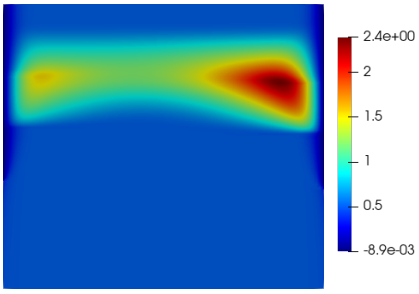

(a) Phosphate (X) with $k_{X,2} \times 1.2$

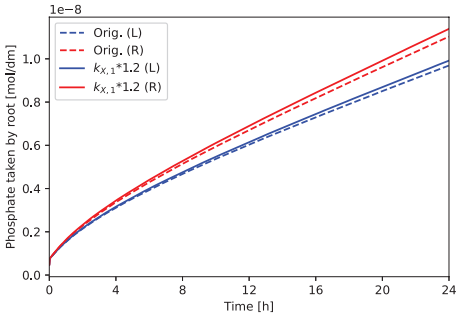

(b) Cumulative uptake of phosphate by the left (L) and right (R) root with $k_{X,1} \times 1.2$

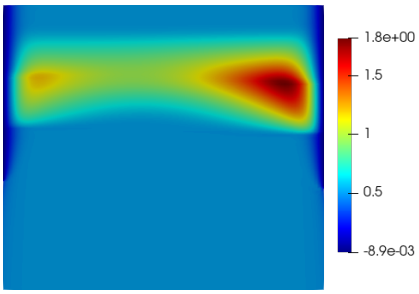

(c) Phosphate (X) with $k_{X,2} \times 0.8$

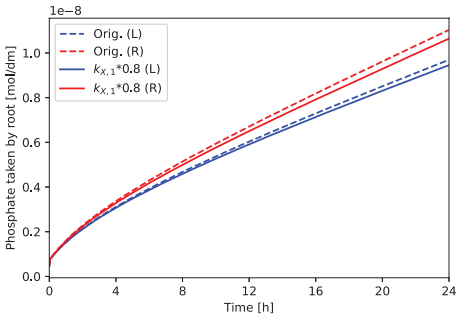

(d) Cumulative uptake of phosphate by the left (L) and right (R) root with $k_{X,2} \times 0.8$

Figure 24: Change in interaction coefficients $k_{X,1}$ and $k_{X,2}$ (with $k_{X,1} = k_{X,2}/5$). In (a) and (c) concentration of phosphate between the two roots after 24 hours in µM; (b) and (d) comparison of phosphate absorbed by each of the roots with original and changed parameters.

the plants happens within 24 hours and therefore intercropping has no effect in that time frame. However, locating the roots at smaller distances apart enables exudates to diffuse from one root to the other, which makes more nutrient available closer to both roots. Therefore, if there is information on the radii of zones of root influence of both plants, it is easy to calculate a maximal distance between the two roots that is necessary to achieve interaction resulting in the two roots benefiting from each other.

Next, we compared nutrient uptake with roots placed at larger distance with original and increased exudation rate. Although we found that even with the roots further apart more nutrient was taken up by having more exudation, the value for what minimal exudation rate is necessary to achieve this effect needs to be further studied. We also tried increasing nutrient absorption power which also resulted in more nutrient absorbed by the root, however, how much is absorbed is limited by the amount of nutrient available in the rhizosphere which depends on the amount of exudate in the soil, i.e. on the exudation rate. We therefore identify the exudation rate of the plant and root distance with intersecting the zones of root influence as two of the main factors necessary for beneficial intercropping.

In section 5.2 we proceeded with further numerical experiments with the extended model, i.e. a system with two different plants, each of which secretes two (same) exudates. To start with, we simulated a scenario where one of the exudates gets consumed in the soil by microbes. As expected, this indeed decreased uptake of the nutrient, therefore ideally the plants should be grown at conditions with minimal biodegradation. We further experimented with increasing the uptake power in this model with the same conclusions as in section 3.4.

Experiments with buffer powers have shown interesting results as well. First, we found that large nutrient buffer power enhances nutrient uptake by the roots. We presented an attempt to justify this result by expressing the buffer power as a ratio between the adsorption and desorption rate. We assumed that increased adsorption rate causes more P to stick on the soil particles from where citrate (one of the exudates) pushes it into the soil solution which is followed by its solubilisation by phytase (the other exudate), thus

		Absorbed phosphate [$\mathrm{mol\,dm^{-1}}$]		Change	
Num. experiment	**Parameter change**	**Left root**	**Right root**	**Left root**	**Right root**
Benchmark solution	Base parameters	9.689×10^{-9}	1.103×10^{-8}	-	-
Citrate biodegradation	$V_{\max} = 2.5 \times 10^{-9}$	9.409×10^{-9}	1.047×10^{-8}	-2.9%	-5.08%
Uptake power	$\alpha_1 \times 10$	1.188×10^{-8}	1.103×10^{-8}	22.6%	0.00%
Uptake power	$\alpha_1 / 10$	9.087×10^{-9}	1.103×10^{-8}	-6.2%	0.00%
Phosphate buffer power	$b_X \times 2$	1.521×10^{-8}	1.806×10^{-8}	57.0%	63.74%
Phosphate buffer power	$b_X / 2$	6.495×10^{-9}	7.095×10^{-9}	-33.0%	-35.68%
Phytase buffer power	$b_{Y,1} \times 2$	9.593×10^{-9}	1.097×10^{-8}	-1.0%	-0.54%
Phytase buffer power	$b_{Y,1} / 2$	9.810×10^{-9}	1.110×10^{-8}	1.2%	0.63%
Citrate buffer power	$b_{Y,2} \times 2$	9.416×10^{-9}	1.045×10^{-8}	-2.8%	-5.26%
Citrate buffer power	$b_{Y,2} / 2$	1.004×10^{-8}	1.166×10^{-8}	3.6%	5.71%
Diffusion coefficients	$D_{L,X} \times 1.2$	1.054×10^{-8}	1.198×10^{-8}	8.8%	8.61%
Diffusion coefficients	$D_{L,Y,1} \times 1.2$	9.669×10^{-9}	1.102×10^{-8}	-0.2%	-0.09%
Diffusion coefficients	$\{D_{L,Y,1}, D_{L,Y,2}\} \times 1.2$	9.619×10^{-9}	1.091×10^{-8}	-0.7%	-1.09%
Diffusion coefficients	$\{D_{L,X}, D_{L,Y,1}, D_{L,Y,2}\} \times 1.2$	1.047×10^{-8}	1.186×10^{-8}	8.1%	7.52%
Exudation rate	$F_{Y,1,1} \times 10$	1.187×10^{-8}	1.114×10^{-8}	22.5%	1.00%
Exudation rate	$F_{Y,1,1} \times 10$ and $D_{L,Y,1} \times 1.2$	1.173×10^{-8}	1.117×10^{-8}	21.1%	1.27%
Exudation rate	$F_{Y,1,1} \times 10$ and $D_{L,X} \times 1.2$	1.288×10^{-8}	1.210×10^{-8}	32.9%	9.70%
Exudation rate	$F_{Y,1,1} \times 10$ and $\{D_{L,X}, D_{Y,1}\} \times 1.2$	1.273×10^{-8}	1.214×10^{-8}	31.4%	10.06%
Exudation rate	$F_{Y,1,1} \times 10$ and $w/2$	2.423×10^{-8}	2.374×10^{-8}	150.1%	115.23%
Distance	$w/2$	1.997×10^{-8}	2.231×10^{-8}	106.1%	102.27%
Interaction coefficients	$k_{X,1} \times 1.2$	9.914×10^{-9}	1.138×10^{-8}	2.3%	3.17%
Interaction coefficients	$k_{X,1} \times 0.8$	9.451×10^{-9}	1.064×10^{-8}	-2.5%	-3.54%

Table 5: Total phosphate absorbed in each of the roots after 24 hours and relative change of resulting values with respect to results obtained by using the original (base) parameters defined in Table 2.

making more phosphate (the nutrient) available for the root. When experimenting with different values for the buffer power of the exudates, we found the exact opposite behaviour compared to the effects of change in nutrient buffer power. We discovered that smaller buffer power of the exudates is necessary to increase nutrient absorption into the root. In this case decreasing the exudate buffer power was explained as causing the exudates to not stick to the soil particles that much, allowing them to move into the soil solution and making more nutrient available in the rhizosphere.

Upon the findings about the buffer power and their effect on the transport of the chemicals in the rhizosphere, we decided to examine the effect of increasing the diffusion coefficients in free solution. We found that although increased diffusion of the nutrient indeed helps the root to access it more easily, the opposite holds for increasing diffusion coefficients of the exudates. With the exudates diffusing away from the root, the nutrient becomes available further away from the root as well and thus it takes the nutrient longer to get to the root. Although not captured by the parameter set-up we experimented with, the delay of the nutrient in reaching the root might also cause more biodegradation of the nutrient which would have a negative effect on nutrient uptake. We must also note that we experimented only with diffusion coefficient in free solution and that the actual diffusion coefficient is calculated as its product with water volume fraction and diffusion impedance factor. However, the results can also be generalised to the diffusion coefficient itself, e.g. diffusion is increased when there is more water content in the soil.

Next, we again explored the effect of combining increased exudation rate with a smaller root distance, and with increased diffusion coefficients. In agreement with the findings in section 3.4 we have shown that much more nutrient is taken by the root with larger exudation rate and smaller distance. We also found that although combining increased exudation rate with increased diffusion coefficient of the same exudate resulted in more nutrient uptake compared to the benchmark solution, better result was obtained without an increase in diffusion which is in accordance with findings presented in the previous paragraph. Also, increasing both the exudation rate and diffusion rate of the nutrient achieved more nutrient uptake than

with only an increase in exudation rate, likewise explained in the previous paragraph.

Finally, we experimented with interaction coefficients, trying to understand their meaning in the model. We found that when we increase the coefficients, more nutrient is absorbed by the root. In order to try to make sense of this result we must notice that increasing the interaction coefficient means increasing nutrient desorption from soil solid into soil solution which makes more nutrient available in the rhizosphere.

One of the characteristics we have not experimented with is the root growth rate. However, we may expect that if the there is a significant difference between the growth rates of the two plants grown next to each other, their zones of root influence will eventually move too far away for the plants to actively benefit from each other. However, this probably depends on the particular plants chosen for intercropping.

In the above, we have summarised the main findings in this report. We described what changes in root or soil characteristics resulted in increased nutrient uptake in a model for intercropping where two plants are grown next to each other for their mutual benefit. Thus, when choosing suitable plants and soil conditions for intercropping, special care should be given to the parameters that enhance nutrient uptake highlighted in this section. Although the mathematical model that we used in this project has its limitations due to many assumptions we have made, it can still be considered to give an approximate idea about what is actually happening in the soil, without the effort, cost and technology it would take to perform these experiments in laboratory conditions.

7 Existence of Solutions

Taking into account the extensions of the original system from [6], a more general version of system (2.3) is studied in this section.

Let $\Omega \subset \mathbb{R}^2$ be a rectangular domain, where we identify $\Gamma := \partial\Omega$. Let $Q := \Omega \times (0,T)$ for some fixed time $T > 0$. Here, let $y(x,t)$ and $s(x,t)$ be vector functions from $\Omega \times [0,T]$ in $\mathbb{R}^n$ where for convenience we write $x = (r,z) \in \Omega$ and also $\Sigma = \Gamma \times (0,T)$. For each $\ell \in [\![1,n]\!]$, let us define the uniformly elliptic operator L^ℓ as

$$L^\ell y^\ell = \nabla \cdot (a^\ell \nabla y^\ell) + b^\ell \cdot \nabla y^\ell = \sum_{i=1}^{2}\sum_{j=1}^{2} \frac{\partial}{\partial x_i}\left(a^\ell_{i,j}\frac{\partial}{\partial x_j} y^\ell\right) + \sum_{i=1}^{2} b^\ell_i \frac{\partial}{\partial x_i} y^\ell,$$

where a^ℓ, $b^\ell \in L^\infty(Q)$, with a^ℓ a matrix such that $a^\ell_{i,i} \geq 0$ and $\xi^\top (a^\ell(x,t)\xi) \geq \Theta|\xi|^2$ for some $\Theta > 0$ and all $(x,t) \in Q$, $\xi \in \mathbb{R}^2$. Moreover, let $F : \mathbb{R}^n \to \mathbb{R}^n$ such that each component F^ℓ belongs to $C^1(\mathbb{R}) \cap L^\infty(\mathbb{R})$, is Lipschitz continuous, and non negative for non negative arguments, and let $h \in L^2(\mathbb{R}^n, [0,T])$ affine on y, and such that $h(0,t) \leq M$ for all t. Now, let $G \in C^\infty(\mathbb{R}^{n+1}, \mathbb{R}^n)$ be bilinear such that each $G^\ell(s,\cdot)$ is linear in y for fixed s, and each $G^\ell(\cdot, y)$ depends linearly only on s^ℓ for fixed y. Also, we assume that $-G$ has the positiveness property that $-G^\ell(0,y) \geq 0$ if $y \geq 0$ component-wise. We will present a precise form for h and G later. Finally, let the initial conditions be $y_0, s_0^\ell \in L^\infty(\Omega)$ and non-negative.

We look after the solution of the system

$$\frac{\partial}{\partial t} y^\ell = L^\ell y^\ell - y^\ell F^\ell(y^\ell) + G^\ell(s^\ell, y^1, \dots y^n) \qquad \text{in } Q, \forall \ell \in [\![1,n]\!], \tag{7.1a}$$

$$\frac{\partial}{\partial t} s^\ell = -G^\ell(s^\ell, y^1, \dots y^n) \qquad \text{in } Q, \forall \ell \in [\![1,n]\!], \tag{7.1b}$$

$$(a^\ell \nabla y^\ell + y^\ell b^\ell) \cdot \vec{n} = h^\ell(y^\ell, x, t) \qquad \text{on } \Sigma, \forall \ell \in [\![1,n]\!], \tag{7.1c}$$

$$y^\ell(0) = y_0^\ell \qquad \text{in } \Omega, \forall \ell \in [\![1,n]\!], \tag{7.1d}$$

$$s^\ell(0) = s_0^\ell \qquad \text{in } \Omega, \forall \ell \in [\![1,n]\!]. \tag{7.1e}$$

Here the set $[\![1,n]\!]$ is just the integer interval with extremes 1 and n, namely

$$[\![1,n]\!] = \{1,2,\dots,n-1,n\}.$$

We are interested in particular for G to be in the form

$$G^\ell(s^\ell, y) = \beta_0^\ell s^\ell - \gamma^\ell y^\ell + \sum_{\substack{1\le i\le n\\ i\neq \ell}} \beta_i^\ell y^i s^\ell, \tag{7.2}$$

where for the positivity assumption we will require $\gamma^\ell > 0$. We will further assume that $\beta_i^\ell \geq 0$ for all $i \in [\![1,n]\!] \setminus \{\ell\}$ and $\beta_0^\ell \geq 0$. Similarly, each component of h can be written as

$$h^\ell(y^\ell, x, t) = \alpha^\ell(x,t)y^\ell + \nu^\ell(x,t), \tag{7.3}$$

with ν^ℓ a bounded function, and both α^ℓ and ν^ℓ integrable. Without loosing generality, let us assume further that α^ℓ and ν^ℓ are continuous and that α^ℓ is bounded as well. Finally, let us assume that $\nu^\ell \geq 0$.

7.1 Analysis of the general coupled system

In this section we will follow a similar procedure as [22, 20, 23], and [24] to determine and study a solution of coupled PDE-ODE systems. The scheme is as follows: (a) Show that for fixed y there is a unique solution of the ODE system. (b) Show that for fixed s and a linearisation on y there is a unique solution of the PDE system. (c) Show that the mapping that takes an initial y and solves the decoupled ODE-PDE system has a fixed point. Along this procedure the boundedness of solutions as well as their non negativity will be shown.

Let us begin defining the convex subspace of $(L^2(Q))^n$:

$$Y = \left\{ y \in (L^2(Q))^n : 0 \leq y(x,t) \leq \vartheta \quad \text{for a.e.} \quad (x,t) \in Q \right\}$$

for a fixed $\vartheta > 0$. The existence of a solution of (7.1) is equivalent to the existence of a fixed point of K defined on Y by $y_m = K(y_{m-1})$, where y_m is a solution of the system

$$\frac{\partial}{\partial t} y_m^\ell = L^\ell y_m^\ell - y_m^\ell F^\ell(y_{m-1}^\ell) + G^\ell(s_m^\ell, y_m^1, \dots y_m^n) \qquad \text{in } Q, \forall \ell \in [\![1,n]\!], \tag{7.4a}$$

$$\frac{\partial}{\partial t} s_m^\ell = -G^\ell(s_m^\ell, y_{m-1}^1, \dots y_{m-1}^n) \qquad \text{in } Q, \forall \ell \in [\![1,n]\!], \tag{7.4b}$$

$$(a^\ell \nabla y_m^\ell + y_m^\ell b^\ell) \cdot \vec{n} = h^\ell(y_m^\ell, x, t) \qquad \text{on } \Sigma, \forall \ell \in [\![1,n]\!], \tag{7.4c}$$

$$y_m^\ell(0) = y_0^\ell \qquad \text{in } \Omega, \forall \ell \in [\![1,n]\!], \tag{7.4d}$$

$$s_m^\ell(0) = s_0^\ell \qquad \text{in } \Omega, \forall \ell \in [\![1,n]\!]. \tag{7.4e}$$

Now we can divide the system in two parts. First, the analysis of the differential equations (7.4b), and then the analysis for the partial differential equations in (7.4a).

(A) Subsystem of ordinary differential equations

Observe that for any given $y_{m-1} \in Y$, then the ODE system (7.4b)–(7.4e) is a non-homogeneous linear system of ordinary differential equations. Carathéodory's theorem gives us that there exists a unique solution $s_m \in H^1(0,T;(L^2(\Omega))^n)$ for some T. We can improve this regularity. Recalling (7.2), for any $y_{m-1} \in Y$,

$-G(s_m, y_{m-1})$ can be written as

$$-G(s_m, y_{m-1}) = B(y_{m-1})s_m + C(y_{m-1})$$

with C a vector and B a diagonal matrix. As $B(y)(t_1)$ commutes with $B(y)(t_2)$, for any $t_1, t_2 \in \mathbb{R}$ (as it is a diagonal matrix), we further have that there is a $H^1(0,T;(L^2(\Omega))^n)$ solution given by

$$s_m(t) = e^{\overline{B}(t)}s_0 + \int_0^t e^{\overline{B}(t)-\overline{B}(r)}C(y_{m-1})\,\mathrm{d}r$$

with $\overline{B}(t) = \int_0^t B(y_{m-1})(\xi)\,\mathrm{d}\xi$ [25]. Particularly, each row of s_m will be given exactly by

$$s_m^\ell(t) = s_0\, e^{\int_0^t B_{\ell,\ell}(y_{m-1})(\xi)\,\mathrm{d}\xi} + \int_0^t e^{\int_0^t B_{\ell,\ell}(y_{m-1})(\xi)\,\mathrm{d}\xi - \int_0^r B_{\ell,\ell}(y_{m-1})(\xi)\,\mathrm{d}\xi} C^\ell(y_{m-1})(r)\,\mathrm{d}r. \tag{7.5}$$

Here we have that

$$B_{\ell,\ell} = -\beta_0^\ell - \sum_{\substack{1\le i\le n\\ i\neq\ell}} \beta_i^\ell y_{m-1}^i \qquad \text{and} \qquad C^\ell(y_{m-1}) = \gamma^\ell y_{m-1}^\ell,$$

where we have to recall that $\gamma_i^\ell \geq 0$ and $y_{m-1} \in Y$. As a result, (7.5) yields an always non negative solution $s_m \in L^\infty(Q)$. If we did not have a closed expression for s_m, we could have argued via the work of [26] on positiveness for ODE systems, which requires the positiveness assumption for $-G$ and s_0. In any case, we have got that $s_m^\ell \in H^1(0,T;L^2(\Omega)) \cap L^\infty(Q)$ and $s_m^\ell \geq 0$ for each $\ell \in [\![1,n]\!]$ whenever $y_{m-1} \in Y$.

(B) Subsystem of partial differential equations

Next we turn to the linear system (7.4a), (7.4c), (7.4d) of parabolic differential equations. Further, as we already have s_m, it is now *decoupled* from the ODE system.

We say that a vector function y_m is a weak solution of (7.4a) with boundary conditions (7.4c) and initial conditions (7.4d) if each $y_m^\ell \in L^2(0,T;H^1(\Omega))$ and $\frac{\partial y_m^\ell}{\partial t} \in L^2(0,T;(H^1(\Omega))^*)$ satisfy

$$\begin{aligned}\int_0^T \left\langle \frac{\partial y_m^\ell}{\partial t}, v\right\rangle \mathrm{d}t = &-\int_0^T\int_\Omega (a^\ell \nabla y_m^\ell + y_m^\ell b^\ell)\cdot\nabla v\,\mathrm{d}x\,\mathrm{d}t + \int_0^T\int_\Gamma h^\ell(y_m^\ell, x, t)v\,\mathrm{d}\sigma\,\mathrm{d}t\\ &+\int_0^T\int_\Omega -y_m^\ell F^\ell(y_{m-1}^\ell)v + G^\ell(s_m^\ell, y_{m-1})v\,\mathrm{d}x\,\mathrm{d}t\end{aligned} \tag{7.6}$$

for all $v \in L^2(0,T;H^1(\Omega))$, and with the initial condition $y_m^\ell \to y_0^\ell$ in $L^2(\Omega)$ as $t \to 0$, for all $\ell \in [\![1,n]\!]$. Here we have used the duality pairing $\langle\cdot,\cdot\rangle$ of $(H^1(\Omega))^*$ and $H^1(\Omega)$.

Problem (7.6) has been extensively studied in the literature, see for example [27] or [28]. Using Galerkin's method, we can prove that there is a unique solution given component-wise as the element $y_m^\ell \in L^2(0,T;H^1(\Omega)) \cap L^\infty(0,T;L^2(\Omega))$ with $\frac{\partial y_m^\ell}{\partial t} \in L^2(0,T;(H^1(\Omega))^*)$.

Proof of existence of y_m

We will adapt ideas from [27, 29] and [16].

Consider a fundamental system of functions $(w_k)_{k\in\mathbb{N}^*}$ in $H^1(\Omega)$; i.e., they form an orthogonal basis in $H^1(\Omega)$, and for simplicity let us assume further that they are orthonormalised in $L^2(\Omega)$. Moreover, let us

define[§]

$$a^\ell[y_m, v; t] := \int_\Omega (a^\ell \nabla y_m^\ell + y_m^\ell b^\ell) \cdot \nabla v \,\mathrm{d}x + \int_\Omega d^\ell(y_m) v \,\mathrm{d}x - \int_\Gamma \alpha^\ell(x,t) y_m^\ell v \,\mathrm{d}\sigma$$

where we have used the explicit form of h^ℓ presented in (7.3), and d^ℓ is given by

$$d^\ell(y_m) := y_m^\ell F^\ell(y_{m-1}^\ell) + \gamma^\ell y_m^\ell - s_m^\ell \sum_{\substack{1\le i\le n \\ i\neq \ell}} \beta_i^\ell y_m^i.$$

Also let us define the two linear functionals in v

$$\mathbf{f}^\ell(t) := \beta_0^\ell \int_\Omega s_m^\ell v \,\mathrm{d}x \qquad \text{and} \qquad \mathbf{g}^\ell(t) := \int_\Gamma \nu^\ell(x,t) v \,\mathrm{d}\sigma.$$

Notice that these are well defined as F^ℓ and s_m^ℓ are bounded.

Fix a positive integer N. We will seek for an approximate solution in the form

$$\mathbf{y}_m^{\ell,N}(t)(x) = \sum_{k=1}^N c_k^{\ell,N}(t) w_k(x) \tag{7.7}$$

so that the coefficients $c_k^{\ell,N}$ are determined by

$$\left(\frac{\partial}{\partial t} y_m^{\ell,N}, w_k\right)_\Omega + a^\ell[y_m^N, w_k; t] = \left(\mathbf{f}^\ell(t), w_k\right)_\Omega + \left(\mathbf{g}^\ell(t), w_k\right)_\Gamma \tag{7.8}$$

for almost every $t \in (0,T)$ with the initial condition $c_k^N(0) = (y^\ell(0), w_k)_\Omega = (y_0^\ell, w_k)_\Omega$ for all $k \in [\![1, N]\!]$; where

$$\begin{aligned} a^\ell[y_m^N, w_k; t] = \sum_{i=1}^N \Bigg[c_i^{\ell,N} \int_\Omega (a^\ell \nabla w_i + w_i b^\ell) \cdot \nabla w_k \,\mathrm{d}x - c_i^{\ell,N} \int_\Gamma \alpha^\ell w_i w_k \,\mathrm{d}\sigma \\ + \int_\Omega c_i^{\ell,N} (w_i F^\ell w_k) + \frac{1}{N} \gamma^\ell c_k^{\ell,N} - \sum_{\substack{1\le j\le n \\ j\neq \ell}} \beta_j^\ell c_i^{j,N} (s_m^\ell w_i w_k) \,\mathrm{d}x \Bigg] =: A^\ell(c^N) \end{aligned}$$

Using orthogonality and orthonormality of $(w_k)_{k\in\mathbb{N}^*}$, we obtain the system

$$\frac{\mathrm{d}}{\mathrm{d}t} c_k^{\ell,N} + A^\ell(c^N) = l_k^\ell(t) \tag{7.9a}$$

$$c_k^{\ell,N}(0) = (y_0^\ell, w_k) \tag{7.9b}$$

for almost every $t \in (0,T)$, all $k \in [\![1,N]\!]$, and $n \in [\![1,n]\!]$; with the functions $l_k^\ell(t) = \left(\mathbf{f}^\ell(t), w_k\right)_\Omega + \left(\mathbf{g}^\ell(t), w_k\right)_\Gamma$.

The system (7.9) is a system of linear ordinary differential equations in terms of $c_k^{\ell,N}$ with initial value conditions. Owing to Carathèodory's theorem, there exists a unique solution $c^N \in \left(H^1(0,T)\right)^{nN}$. Now, if

[§]Notice that a^ℓ is linear in y_m, not only in y_m^ℓ.

we put $c^{\ell,N}$ as a test function in (7.8) and sum over k, we get that

$$\Big(\frac{\partial}{\partial t}y_m^{\ell,N}, y_m^{\ell,N}\Big)_\Omega + a^\ell[y_m^N, y_m^{\ell,N}; t] = \Big(\mathbf{f}^\ell(t), y_m^{\ell,N}\Big)_\Omega + \Big(\mathbf{g}^\ell(t), y_m^{\ell,N}\Big)_\Gamma \tag{7.10}$$

for almost every $t \in (0,T)$ and all $\ell \in [\![1,n]\!]$.

Now, for an arbitrary but fixed $\tau \in (0,T]$ and any $\ell \in [\![1,n]\!]$, we have the identity

$$\int_0^\tau \Big(\frac{\partial}{\partial t}y_m^{\ell,N}(t), y_m^{\ell,N}(t)\Big)_\Omega \,\mathrm{d}t = \frac{1}{2}\int_0^\tau \frac{\partial}{\partial t}\|y_m^{\ell,N}(t)\|_\Omega^2 \,\mathrm{d}t = \frac{1}{2}\|y_m^{\ell,N}(\tau)\|_\Omega^2 - \frac{1}{2}\|y_m^{\ell,N}(0)\|_\Omega^2.$$

If we integrate (7.10) over $[0,\tau]$ and incorporate this last identity, we get that for any $\ell \in [\![1,n]\!]$ it holds

$$\frac{1}{2}\|y_m^{\ell,N}(\tau)\|_\Omega^2 + \int_0^\tau a^\ell[y_m^N, y_m^{\ell,N}; t]\,\mathrm{d}t = \frac{1}{2}\|y_m^{\ell,N}(0)\|_\Omega^2 + \int_0^\tau \Big(\mathbf{f}(t), y_m^{\ell,N}(t)\Big)_\Omega + \Big(\mathbf{g}(t), y_m^{\ell,N}(t)\Big)_\Gamma \,\mathrm{d}t. \tag{7.11}$$

Additionally, by Bessel's inequality, we have that

$$\|y_m^{\ell,N}(0)\|_\Omega^2 = \sum_{k=1}^N |c_k^{\ell,N}(0)|^2 = \sum_{k=1}^N |(y_0^\ell, w_k)|^2 \leq \|y_0^\ell\|_\Omega^2. \tag{7.12}$$

Moreover, it is not hard to show, using Cauchy's inequality, that for any element $v \in (H^1(\Omega))^n$ the inequality

$$\frac{1}{2}\Theta\|\nabla v^\ell\|_\Omega^2 \leq a^\ell[v, v^\ell; t] + \frac{1}{2}C_{s,b,\alpha,F}^\ell \sum_{k=1}^n \|v^k\|_\Omega^2$$

is satisfied, where $C_{s,b,\alpha,F}^\ell$ is a constant depending linearly on the supremum norms of s_m^ℓ, b^ℓ, α^ℓ, and $F^\ell(y_{m-1}^\ell)$. Furthermore, applying Cauchy's inequality again we get

$$\Big|\Big(\mathbf{f}^\ell, y_m^{\ell,N}\Big)_\Omega\Big| \leq \frac{1}{2}\|\mathbf{f}^\ell\|_\Omega^2 + \frac{1}{2}\|y_m^{\ell,N}\|_\Omega^2 \qquad \text{and} \qquad \Big(\mathbf{g}^\ell, y_m^{\ell,N}\Big)_\Gamma \leq \varepsilon\|\mathbf{g}^\ell\|_\Gamma^2 + \frac{1}{4\varepsilon}\|y_m^{\ell,N}\|_\Gamma^2.$$

This way we can use a proper selection of ε alongside the trace inequality [16] to obtain, for some C_1 and C_2, that

$$\frac{\mathrm{d}}{\mathrm{d}t}\|y_m^{\ell,N}\|_\Omega^2 + \Theta\|\nabla y_m^{\ell,N}\|_\Omega^2 \leq C_1\sum_{k=1}^n \|y_m^{k,N}\|_\Omega^2 + C_2\Big(\|\mathbf{f}^\ell\|_\Omega^2 + \|\mathbf{g}^\ell\|_\Gamma^2\Big).$$

We can sum the inequalities with respect to ℓ to obtain

$$\frac{\mathrm{d}}{\mathrm{d}t}\sum_{\ell=1}^n \|y_m^{\ell,N}\|_\Omega^2 + \Theta\sum_{\ell=1}^n \|\nabla y_m^{\ell,N}\|_\Omega^2 \leq C_1\sum_{\ell=1}^n \|y_m^{\ell,N}\|_\Omega^2 + C_2\sum_{\ell=1}^n \Big(\|\mathbf{f}^\ell\|_\Omega^2 + \|\mathbf{g}^\ell\|_\Gamma^2\Big), \tag{7.13}$$

with updated C_1 and C_2. Notice that this is a differential inequality, so we can use Grönwall's inequality [16] to get the estimate

$$\sum_{\ell=1}^n \|y_m^{\ell,N}(t)\|_\Omega^2 \leq \sum_{\ell=1}^n e^{C_1 t}\left(\|y_m^{\ell,N}(0)\|_\Omega^2 + C_2\int_0^t \|\mathbf{f}^\ell(r)\|_\Omega^2 + \|\mathbf{g}^\ell(r)\|_\Gamma^2\,\mathrm{d}r\right). \tag{7.14}$$

Now, by (7.12) and the fact that (7.14) is a sum of positive terms, we get the particular estimate

$$\max_{0\le t\le T}\|y_m^{\ell,N}(t)\|_\Omega^2 \le C\sum_{k=1}^{n}\left(\|y_0^k\|_\Omega^2+\|\mathbf{f}^k\|^2_{L^2(0,T;L^2(\Omega))}+\|\mathbf{g}^k\|^2_{L^2(0,T;L^2(\Gamma))}\right) \tag{7.15}$$

for each $\ell\in[\![1,n]\!]$.

Now we can use (7.11) replacing τ with T, estimate (7.13) completing the H^1–norm of each $y_m^{\ell,N}$, and estimate (7.15) to get

$$\|y_m^{\ell,N}\|^2_{L^2(0,T,H^1(\Omega))} \le C\sum_{k=1}^{n}\left(\|y_0^k\|_\Omega^2+\|\mathbf{f}^k\|^2_{L^2(0,T,L^2(\Omega))}+\|\mathbf{g}^k\|^2_{L^2(0,T,L^2(\Gamma))}\right),$$

where C is a generic positive constant. With these estimates we have got that

$$\|y_m^{\ell,N}\|^2_{L^\infty(0,T;L^2(\Omega))}+\|y_m^{\ell,N}\|^2_{L^2(0,T;H^1(\Omega))} \le C\sum_{k=1}^{n}\left(\|y_0^k\|_\Omega^2+\|\mathbf{f}^k\|^2_{L^2(0,T;L^2(\Omega))}+\|\mathbf{g}^k\|^2_{L^2(0,T;L^2(\Gamma))}\right);$$

where the term on the right-hand side is a constant independent of N, let us call it K_m. Observe that in particular (7.15) yields $\|y_m^{\ell,N}(t)\|_\Omega^2\le K_m$ for all $t\in[0,T]$, and in view of the orthonormality

$$\sum_{k=1}^{N}|c_k^N(t)|^2\le K_m \tag{7.16}$$

for all $t\in[0,T]$ and $N\in\mathbb{N}^*$.

We can even go a step further. Fix any $v\in H^1(\Omega)$ with $\|v\|_{H^1(\Omega)}\le 1$ and write it as $v=v^1+v^2$, where v^1 is generated by the span of $\{w_k\}_{k=1}^N$ and $(v^2,w_k)=0$ for all $k\in\{1,\dots,N\}$. Since the functions $(w_k)_{k\in\mathbb{N}^*}$ are orthogonal in $H^1(\Omega)$, we get $\|v^1\|_{H^1(\Omega)}\le\|v\|_{H^1(\Omega)}\le 1$. Utilising (7.8), we get that for almost every $t\in(0,T)$

$$\left(\frac{\partial}{\partial t}y_m^{\ell,N},v^1\right)_\Omega+a^\ell[y_m^N,v^1;t]=\left(\mathbf{f}^\ell(t),v^1\right)_\Omega+\left(\mathbf{g}^\ell(t),v^1\right)_\Gamma.$$

Then (7.7) implies

$$\left\langle\frac{\partial}{\partial t}y_m^{\ell,N},v\right\rangle=\left(\frac{\partial}{\partial t}y_m^{\ell,N},v\right)_\Omega=\left(\frac{\partial}{\partial t}y_m^{\ell,N},v^1\right)_\Omega=\left(\mathbf{f}^\ell(t),v^1\right)_\Omega+\left(\mathbf{g}^\ell(t),v^1\right)_\Gamma-a^\ell[y_m^N,v^1;t].$$

Continuity of a^ℓ and the norm of v with by Cauchy–Bunyakovsky–Schwarz inequality give

$$\left|\left\langle\frac{\partial}{\partial t}y_m^{\ell,N},v\right\rangle\right|\le C\sum_{k=1}^{n}\left(\|\mathbf{f}^k\|_\Omega+\|\mathbf{g}^k\|_\Gamma+\|y_m^{k,N}\|_{H^1(\Omega)}\right);$$

thus the operator norm of $\frac{\partial}{\partial t}y_m^{\ell,N}$ is bounded for almost everywhere $t\in(0,T)$. Additionally, we can square the last inequality, use again Cauchy's inequality and get

$$\left\|\frac{\partial}{\partial t}y_m^{\ell,N}\right\|_{(H^1(\Omega))^*}\le C\sum_{k=1}^{n}\left(\|\mathbf{f}^k\|_\Omega+\|\mathbf{g}^k\|_\Gamma+\|y_m^{k,N}\|_{H^1(\Omega)}\right);$$

and therefore

$$\int_0^T \left\| \frac{\partial}{\partial t} y_m^{\ell,N} \right\|^2_{(H^1(\Omega))^*} \mathrm{d}t \leq C \sum_{k=1}^{n} \left(\|y_0^k\|^2_\Omega + \|\mathbf{f}^k\|^2_{L^2(0,T,L^2(\Omega))} + \|\mathbf{g}^k\|^2_{L^2(0,T,L^2(\Gamma))} \right).$$

As a result, we have got

$$\begin{aligned} \|y_m^{\ell,N}\|^2_{C([0,T];L^2(\Omega))} + \|y_m^{\ell,N}\|^2_{L^2(0,T;H^1(\Omega))} + \|\partial_t y_m^{\ell,N}\|^2_{L^2(0,T;H^1(\Omega)^*)} \\ \leq C \sum_{k=1}^{n} \left(\|y_0^k\|^2_\Omega + \|\mathbf{f}^k\|^2_{L^2(0,T;L^2(\Omega))} + \|\mathbf{g}^k\|^2_{L^2(0,T;L^2(\Gamma))} \right). \end{aligned} \tag{7.17}$$

According to the energy estimates (7.17) and (7.16), we see that $(y_m^{\ell,N})_{N\in\mathbb{N}^*}$ is bounded in $L^2(0,T;H^1(\Omega))$, $(\partial_t y_m^{\ell,N})_{N\in\mathbb{N}^*}$ is bounded in $L^2(0,T;H^1(\Omega)^*)$, and all $c_k^{\ell,N}(t)$ are essentially bounded for all ℓ, k, N, and t. Consequently, there exists a subsequence $(y_m^{\ell,N_q})_{N_q\in\mathbb{N}}$ and functions $y_m^\ell \in L^2(0,T;H^1(\Omega))$, with $\frac{\partial}{\partial t} y_m^\ell \in L^2(0,T;(H^1(\Omega))^*)$ for each $\ell \in [\![1,n]\!]$, such that

$$\begin{cases} y_m^{\ell,N_q} \rightharpoonup y_m^\ell & \text{weakly in } L^2(0,T;H^1(\Omega)), \\ \frac{\partial}{\partial t} y_m^{\ell,N_q} \rightharpoonup \frac{\partial}{\partial t} y_m^\ell & \text{weakly in } L^2(0,T;H^1(\Omega)^*). \end{cases} \tag{7.18}$$

Moreover, owing to the weak lower sequential semicontinuity of the norm, we also get that $\|y_m^\ell(t)\|_\Omega$ is also bounded by K_m for all $t \in [0,T]$, thus $y_m^\ell \in L^\infty(0,T;L^2(\Omega))$.

Now, for a fixed integer $\tilde{n}$, let us pick a function $\mathbf{v} \in C^1([0,T];H^1(\Omega))$ of the form

$$\mathbf{v}(t) = \sum_{k=1}^{\tilde{n}} d_k(t) w_k, \tag{7.19}$$

with $\{d_k\}_{k=1}^{\tilde{n}}$ a set of given functions. Let us pick $N \geq \tilde{n}$, multiply (7.8) by c_k, sum over k and then integrate with respect to t to find

$$\int_0^T \left\langle \frac{\partial}{\partial t} y_m^{\ell,N}, \mathbf{v} \right\rangle + a^\ell[y_m^N, \mathbf{v}; t] \,\mathrm{d}t = \int_0^T \left(\mathbf{f}^\ell(t), \mathbf{v} \right)_\Omega + \left(\mathbf{g}^\ell(t), \mathbf{v} \right)_\Gamma \mathrm{d}t.$$

Using the subsequence and recalling (7.18) and taking limit $N \to \infty$, we get

$$\int_0^T \left\langle \frac{\partial}{\partial t} y_m^{\ell}, \mathbf{v} \right\rangle + a^\ell[y_m^\ell, \mathbf{v}; t] \,\mathrm{d}t = \int_0^T \left(\mathbf{f}^\ell(t), \mathbf{v} \right)_\Omega + \left(\mathbf{g}^\ell(t), \mathbf{v} \right)_\Gamma \mathrm{d}t. \tag{7.20}$$

This equality then holds for all functions $\mathbf{v} \in L^2(0,T;H^1(\Omega))$, as functions of the form (7.19) are dense in this space.

To prove that $y_m^\ell(0) = y_0^\ell$ it suffices to see that (7.10) can be integrated by parts in time for all $\mathbf{v} \in C^1(0,T;H^1(\Omega))$ with $\mathbf{v}(T) = 0$ [16]. Again passing through a subsequence, noticing that $y_m^{\ell,N_k}(0) \to y_0^\ell$ in $L^2(\Omega)$, and that $\mathbf{v}(0)$ is arbitrary, then we obtain the desired property.

As discussed in [16], uniqueness follows from showing that if y_m^ℓ and u are two solutions of the parabolic problem, then their difference v^ℓ satisfies $\frac{1}{2}\frac{\partial}{\partial t}\|v^\ell\|^2_\Omega + a^\ell[v, v^\ell; t] = 0$. The lower bounds of a^ℓ and Gronwall's inequality later imply that $v \equiv 0$.

(C) Notes on the regularity of y_m^ℓ

It is shown in [16], that as $y_m^\ell \in L^2(0,T;H^1(\Omega))$ and $\frac{\partial}{\partial t} y_m^\ell \in L^2(0,T;(H^1(\Omega))^*)$, then we also have $y_m^\ell \in C([0,T];L^2(\Omega))$. This way, the follow estimate holds:

$$\begin{aligned}\|y_m^\ell\|_{C([0,T];L^2(\Omega))} + \|y_m^\ell\|_{L^2(0,T;H^1(\Omega))} + \|\partial_t y_m^\ell\|_{L^2(0,T;H^1(\Omega)^*)} \\ \leq C \sum_{k=1}^{n} \left(\|y_0^k\|_\Omega + \|\mathbf{f}^k\|_{L^2(0,T;L^2(\Omega))} + \|\mathbf{g}^k\|_{L^2(0,T;L^2(\Gamma))} \right),\end{aligned} \tag{7.21}$$

for every $\ell \in [\![1,n]\!]$.

Now we will proceed to show that the solutions y_m are uniformly bounded. To do this, we will be using the framework of invariant rectangles [30, 31]. As pointed out in [24], the theory of bounded invariant rectangles can be applied to problems of the type (7.4) using a regularisation argument.

Let us recall here the linear system of partial differential equations given by (7.4a), (7.4c), and (7.4d), which we include here for clarity:

$$\frac{\partial}{\partial t} y_m^\ell = L^\ell y_m^\ell - y_m^\ell F^\ell(y_{m-1}^\ell) + G^\ell(s_m^\ell, y_m^1, \dots y_m^n) \qquad \text{in } Q, \forall \ell \in [\![1,n]\!], \tag{7.22a}$$

$$(a^\ell \nabla y_m^\ell + y_m^\ell b^\ell) \cdot \vec{n} = h^\ell(y_m^\ell, x, t) \qquad \text{on } \Sigma, \forall \ell \in [\![1,n]\!], \tag{7.22b}$$

$$y_m^\ell(0) = y_0^\ell \qquad \text{in } \Omega, \forall \ell \in [\![1,n]\!]. \tag{7.22c}$$

Now let us introduce the set $\Sigma = \left\{ y \in \mathbb{R}^n : 0 \leq y \leq \vartheta \right\}$. We claim that Σ is an invariant set for (7.22). Let us define $H(y,t)$ as the reaction term of system (7.22); i.e., $H^\ell(y) := -y^\ell F^\ell(y_{m-1}^\ell) + G^\ell(s_m^\ell, y^1, \dots y^n)$. Using the explicit formulae for G, we get

$$H^\ell(y) = -y^\ell F^\ell(y_{m-1}^\ell) + \beta_0^\ell s_m^\ell - \gamma^\ell y^\ell + s_m^\ell \sum_{\substack{1 \leq i \leq n \\ i \neq \ell}} \beta_i^\ell y^i.$$

This is a linear function in terms of y, thus it is Lipschitz continuous in $\mathbb{R}^n$. Moreover, our choice of boundary conditions guarantee that h^ℓ is also Lipschitz continuous for every $\ell \in [\![1,n]\!]$. Further we can express $H(y) = Ay + b$ for suitable A and b, with b always non negative.

Now, we have that $h^\ell(0,x,t) = \nu^\ell(x,t)$, which is positive by the assumptions we made above for (7.3). Also, the non-negativity of s_m and the positivity of β_0 yield

$$H^\ell(y^1, \dots, y^{\ell-1}, 0, y^{\ell+1}, \dots, y^n) = \beta_0^\ell s_m^\ell + s_m^\ell \sum_{\substack{1 \leq i \leq n \\ i \neq \ell}} \beta_i^\ell y^i \geq 0 \tag{7.23}$$

for any $y^i \geq 0$ for $i \neq \ell$. Considering $K^\ell(y) = -y^\ell$, we get that

$$\nabla K^\ell(y)[H]\Big|_{y^\ell = 0} = -\left(\beta_0^\ell s_m^\ell + s_m^\ell \sum_{\substack{1 \leq i \leq n \\ i \neq \ell}} \beta_i^\ell y^i \right) \leq 0$$

for any $y^i \geq 0$ for $i \neq \ell$. We can do this for all $\ell \in [\![1,n]\!]$. Applying the theorem on positive invariant regions, we conclude that $y \geq 0$ component wise.

Now, at ϑ, we get

$$H^\ell(y^1, \dots, y^{\ell-1}, \vartheta, y^{\ell+1}, \dots, y^n) = -\vartheta(F^\ell(y_{m-1}^\ell) + \gamma^\ell) + \beta_0^\ell s_m^\ell + \sum_{\substack{1 \leq i \leq n \\ i \neq \ell}} s_m^\ell \beta_i^\ell y^i.$$

Then if we consider $K^\ell(y) = y^\ell - \vartheta$, we are looking again to have $\nabla K^\ell(y)[H]\Big|_{y^\ell=\vartheta} \leq 0$, for then we can conclude $y \leq \vartheta$. Notice that in such case we need to satisfy the property

$$\beta_0^\ell s_m^\ell + s_m^\ell \sum_{\substack{1\leq i\leq n \\ i\neq \ell}} \beta_i^\ell y^i \leq \vartheta(F^\ell(y_{m-1}^\ell) + \gamma^\ell). \tag{7.24}$$

In the cases $s_m^\ell \equiv 0$ or $\beta \equiv 0$, this is trivial. Let us now assume that $s_m^\ell \neq 0$ and recall that it is bounded from above. For the first term on the left of (7.24), we can ask $\beta_0^\ell s_m^\ell \leq \vartheta\gamma^\ell$ and then require $\vartheta \geq \beta_0^\ell s_m^\ell/\gamma^\ell$. Similarly, we can limit y^i to balance (7.24). This will not generate a contradiction, for we can analyse the reaction terms for s_m^ℓ as well, where non negativity follows from the same arguments as for y^ℓ, and boundedness for a constant η requires $\gamma^\ell y^\ell \leq \eta\left(\beta_0^\ell + \sum_{\substack{1\leq i\leq n \\ i\neq \ell}} \beta_i^\ell y^i\right)$. Thus (7.24) holds and applying the theorem on positive invariant regions, we conclude that $y \leq \vartheta$ component wise.

(D) Existence of a solution for the system

As a result, we have that $y_m \in Y$ and moreover that the mapping K such that $y_m = K(y_{m-1})$ is defined from Y into itself. Moreover, $y_m^\ell \in L^2(0,T;H^1(\Omega))$ with $\frac{\partial}{\partial t} y_m^\ell \in L^2(0,T;(H^1(\Omega))^*)$, and by Lions-Aubin lemma these spaces are compactly embedded in $L^2(Q)$ [32]. Also we have that Y is a convex subset of $(L^2(Q))^n$. Hence, by Schauder fixed-point theorem [33], there exists a fixed point of $K : Y \to Y$, and this fixed point is a weak solution of the original nonlinear coupled problem (7.1). Moreover, this solution is unique which follows from the fact that F is Lipschitz continuous and all y_m are bounded, which ensures that all nonlinear functionals are Lipschitz.

8 Author contributions

As a group we varied what we contributed, all members contributed to both the modelling side and the computational side. All three modelled the first extension of the base model for two roots and one exudate. Karolína and Andrés produced the initial code for computational experimentation. Later Andrés worked on the non-dimensionalised version of the models and wrote code for two roots and one exudate. Karolína derived the extended model for two exudates and extended the non-dimensionalised code to solve this model. Karolína and Liz worked together on planning, performing, and analysing numerical experiments of the models in this work. Liz worked on the biological background of the models. She worked on an extensive literature review that allowed a comprehensive description of the numerical results, while also providing most parameter values (and ranges) for the models. In addition she made sure the description of our model and results was accurate in the biological and chemical context. Andrés and Liz worked together on producing high quality diagrams describing root interaction and dynamics. Andrés also worked on proving the results on existence of solutions for the coupled systems of differential equations, providing further properties regarding positiveness and boundedness of solutions for all the proposed models. He and Karolína also worked on revising the whole project report for consistency within figures and aided on improving the overall presentation of all figures. Karolína presented the conclusions of the project. All contributed to the editing and reviewing of the report.

References

[1] O. Calicioglu, A. Flammini, S. Bracco, *et al.*, "The future challenges of food and agriculture: An integrated analysis of trends and solutions," *Sustainability*, vol. 11, no. 1, p. 1, 2019. DOI: 10.3390/su11010222.

[2] FACT.MR, "Zinc sulphate market, forecast, trend, analysis & competition tracking -global market insights 2020 to 2030," Fact.MR, 2021. [Online]. Available: https://www.factmr.com/report/3663/zinc-sulphate-market.

[3] D. T. Xuan, V. T. Guong, A. Rosling, *et al.*, "Different crop rotation systems as drivers of change in soil bacterial community structure and yield of rice, oryza sativa," *Biology and Fertility of Soils*, vol. 48, no. 2, pp. 217–225, 2011. DOI: 10.1007/s00374-011-0618-5.

[4] L. B. Vysotskaya, A. W. Trekozova, and G. R. Kudoyarova, "Effect of phosphorus starvation on hormone content and growth of barley plants," *Acta Physiologiae Plantarum*, vol. 38, no. 5, 2016. DOI: 10.1007/s11738-016-2127-5.

[5] S. Samreen and S. Kausar, "Phosphorus fertilizer: The original and commercial sources," in. Apr. 2019, ISBN: 978-1-83881-021-4. DOI: 10.5772/intechopen.82240.

[6] M. Ptashnyk, T. Roose, D. L. Jones, *et al.*, "Enhanced zinc uptake by rice through phytosiderophore secretion: A modelling study," *Plant, Cell & Environment*, vol. 34, no. 12, pp. 2038–2046, Aug. 2011. DOI: 10.1111/j.1365-3040.2011.02401.x.

[7] C. D. Giles, A. E. Richardson, B. J. Cade-Menun, *et al.*, "Phosphorus acquisition by citrate- and phytase-exudingnicotiana tabacumplant mixtures depends on soil phosphorus availability and root intermingling," *Physiologia Plantarum*, vol. 163, no. 3, pp. 356–371, 2018. DOI: 10.1111/ppl.12718.

[8] F. Europe, 2021. [Online]. Available: https://www.fertilizerseurope.com/phosphorus-in-food-production/.

[9] S. G. Pallardy, "Chapter 10 - mineral nutrition," in *Physiology of Woody Plants (Third Edition)*, S. G. Pallardy, Ed., Third Edition, San Diego: Academic Press, 2008, pp. 255–285, ISBN: 978-0-12-088765-1. DOI: https://doi.org/10.1016/B978-012088765-1.50011-7. [Online]. Available: https://www.sciencedirect.com/science/article/pii/B9780120887651500117.

[10] G. Haberlandt, *Physiological plant anatomy*. Macmillan and Company, limited, 1914.

[11] A. Canarini, C. Kaiser, A. Merchant, *et al.*, "Root exudation of primary metabolites: Mechanisms and their roles in plant responses to environmental stimuli," *Frontiers in Plant Science*, vol. 10, p. 157, 2019, ISSN: 1664-462X. DOI: 10.3389/fpls.2019.00157. [Online]. Available: https://www.frontiersin.org/article/10.3389/fpls.2019.00157.

[12] H. Purnobasuki, T. Nurhidayati, S. Hariyanto, *et al.*, "Data of root anatomical responses to periodic waterlogging stress of tobacco (nicotiana tabacum) varieties," *Data in Brief*, vol. 20, pp. 2012–2016, 2018. DOI: https://doi.org/10.1016/j.dib.2018.09.046.

[13] D. M. McKay Fletcher, R. Shaw, A. R. Sánchez-Rodríguez, *et al.*, "Quantifying citrate-enhanced phosphate root uptake using microdialysis," *Plant and Soil*, vol. 70, no. 7, 2019. DOI: 10.1007/s11104-019-04376-4.

[14] C. D. Giles, T. S. George, L. K. Brown, *et al.*, "Does the combination of citrate and phytase exudation in nicotiana tabacum promote the acquisition of endogenous soil organic phosphorus?" *Plant and Soil*, vol. 412, no. 1-2, pp. 43–59, 2016. DOI: 10.1007/s11104-016-2884-3.

[15] J. Sundnes, G. T. Lines, X. Cai, *et al.*, *Computing the Electrical Activity in the Heart*. Springer Berlin Heidelberg, 2006. DOI: 10.1007/3-540-33437-8.

[16] L. Evans, *Partial differential equations*. Providence, R.I: American Mathematical Society, 2010, ISBN: 9780821849743.

[17] M. S. Alnæs, J. Blechta, J. Hake, *et al.*, "The fenics project version 1.5," *Archive of Numerical Software*, vol. 3, no. 100, 2015. DOI: 10.11588/ans.2015.100.20553.

[18] H. P. Langtangen and A. Logg, *Solving PDEs in Python: The FEniCS Tutorial I*, ser. Simula SpringerBriefs on Computing. Springer, 2019, ISBN 978-3-319-52462-7.

[19] T. George and K. Ali, personal communication, Mar. 11, 2021.

[20] M. Ptashnyk and T. Roose, "Derivation of a Macroscopic Model for Transport of Strongly Sorbed Solutes in the Soil Using Homogenization Theory," *SIAM Journal on Applied Mathematics*, vol. 70, no. 7, pp. 2097–2118, Jan. 2010. DOI: 10.1137/080729591.

[21] S. Ruiz, N. Koebernick, S. duncan, *et al.*, "Significance of root hairs at the field scale – modelling root water and phosphorus uptake under different field conditions," *Plant Soil*, vol. 70, no. 7, pp. 281–304, 2020. DOI: 10.1007/s11104-019-04308-2.

[22] S. Eisenhofer, "A coupled system of ordinary and partial differential equations modeling the swelling of mitochondria," Ph.D. dissertation, Technischen Universität München, Jan. 2013. [Online]. Available: https://mediatum.ub.tum.de/doc/1129376/1129376.pdf.

[23] A. Marciniak-Czochra and M. Ptashnyk, "Boundedness of Solutions of a Haptotaxis Model," *Mathematical Models and Methods in Applied Sciences*, vol. 20, no. 03, pp. 449–476, Mar. 2010. DOI: 10.1142/s0218202510004301.

[24] M. Ptashnyk and B. Seguin, "Homogenization of a system of elastic and reaction-diffusion equations modelling plant cell wall biomechanics," *ESAIM: Mathematical Modelling and Numerical Analysis*, vol. 50, no. 2, pp. 593–631, Mar. 2016. DOI: 10.1051/m2an/2015073.

[25] D. G. Schaeffer and J. W. Cain, *Ordinary Differential Equations: Basics and Beyond*. Springer New York, 2016. DOI: 10.1007/978-1-4939-6389-8.

[26] Z. Horváth, "Positivity of Runge-Kutta and diagonally split Runge-Kutta methods," *Applied Numerical Mathematics*, vol. 28, no. 2-4, pp. 309–326, Oct. 1998. DOI: 10.1016/s0168-9274(98)00050-6.

[27] O. A. Ladyženskaja, V. A. Solonnikov, and N. N. Ural'ceva, *Linear and Quasi-Linear Equations of Parabolic Type*, ser. Translations of Mathematical Monographs. Providence: American Mathematical Society, 1968, vol. 23, ISBN: 9781470444402.

[28] C. V. Pao, *Nonlinear Parabolic and Elliptic Equations*. Springer US, 1993. DOI: 10.1007/978-1-4615-3034-3.

[29] F. Tröltzsch, *Optimal control of partial differential equations : theory, methods, and applications*. Providence, Rhode Island: American Mathematical Society, 2010, ISBN: 9781470411749.

[30] R. Redlinger, "Invariant sets for strongly coupled reaction-diffusion systems under general boundary conditions," *Archive for Rational Mechanics and Analysis*, vol. 108, no. 4, pp. 281–291, 1989. DOI: 10.1007/bf01052975.

[31] H. F. Weinberger, "Invariant sets for weakly coupled parabolic and elliptic systems," *Rendiconti di Matematica*, vol. 8, no. 6, pp. 295–310, 1975. [Online]. Available: http://citeseerx.ist.psu.edu/viewdoc/download?doi=10.1.1.297.8841&rep=rep1&type=pdf.

[32] J.-P. Aubin, "Un théorème de compacité," *Comptes Rendus Hebdomadaires des Séances de L'Académie des Sciences*, vol. 256, no. 24, pp. 5042–5044, 1963. [Online]. Available: https://gallica.bnf.fr/ark:/12148/bpt6k4006n/f1164.item.r=.zoom#.

[33] E. Zeidler, *Nonlinear Functional Analysis and its Applications I: Fixed-Point Theorems*. Springer New York, Nov. 6, 1998, 936 pp., Translated by Wadsack, P.R., ISBN: 0387909141.

Appendix

A Availability of data, material, and code

All the files and this document are available in the following repository:

`https://github.com/Defining-Good-Neighbours/Report`

All data files generated or analysed during this study are available as additional files in the following repository:

`https://github.com/Defining-Good-Neighbours/Code`

The images presented in this study were either created by the authors, product of internal communication, or cited accordingly from their original sources.

B Parameter values used for numerical experiments

Parameter	Value	Parameter	Value
θ	0.25 $\mathrm{dm}^3\,\mathrm{dm}^{-3}$	f	0.5
ρ	1.2 $\mathrm{kg\,dm}^{-3}$	$D_{L,X}$	9×10^{-8} $\mathrm{dm}^2\,\mathrm{s}^{-1}$
$D_{L,Y,1}$	4.5×10^{-8} $\mathrm{dm}^2\,\mathrm{s}^{-1}$	$D_{L,Y,2}$	2.1×10^{-8} $\mathrm{dm}^2\,\mathrm{s}^{-1}$
ν	0	g_X	0
$g_{Y,1}$	0	$g_{Y,2}$	0
b_X	$\beta_1/\beta_2 = 790.6$	$b_{Y,1}$	1
$b_{Y,2}$	1	$\kappa_{X,1}$	$\kappa_{X,2}/5 = 18.43$ $\mathrm{dm}^3\,\mathrm{mol}^{-1}$
$\kappa_{X,2}$	$\beta_4/\beta_1 = 92.16$ $\mathrm{dm}^3\,\mathrm{mol}^{-1}$	$\kappa_{Y,1}$	0
$\kappa_{Y,2}$	0	α_1, α_2	5.6×10^{-3} $\mathrm{dm\,s}^{-1}$
$F_{Y,1,1}$	2.503×10^{-10} $\mathrm{mol\,dm}^{-2}\,\mathrm{s}^{-1}$	$F_{Y,2,1}$	1.006×10^{-10} $\mathrm{mol\,dm}^{-2}\,\mathrm{s}^{-1}$
$F_{Y,1,2}$	1.316×10^{-10} $\mathrm{mol\,dm}^{-2}\,\mathrm{s}^{-1}$	$F_{Y,2,2}$	2.722×10^{-10} $\mathrm{mol\,dm}^{-2}\,\mathrm{s}^{-1}$
G_1	0.1728 $\mathrm{dm\,day}^{-1}$	G_2	0.2 $\mathrm{dm\,day}^{-1}$
$\delta L_{X,1}, \delta L_{X,2}$	0.2 dm	$\delta L_{Y,1,1}, \delta L_{Y,2,1}$	0.2 dm
$\delta L_{Y,1,1}, \delta L_{Y,2,1}$	0.2 dm	a	0.005 dm
w	0.04 dm		

Table 6: Original parameter values to compute benchmark result in section 5.2.1.

C Non-dimensionalisation of extended model

Similarly as we did in Section 3.2, we will scale the variables of the model appropriately. Again, we introduce the following relations

$$r = \varepsilon_r \hat{r} + a, \qquad z = \varepsilon_z \hat{z}, \qquad t = \varepsilon_t \hat{t}, \qquad X_L = \varepsilon_x \hat{x}, \qquad Y_{L,1} = \varepsilon_{1,y} \hat{y}_1, \qquad Y_{L,2} = \varepsilon_{2,y} \hat{y}_2;$$

where $\varepsilon_r, \varepsilon_z, \varepsilon_t, \varepsilon_x, \varepsilon_{1,y}$, and $\varepsilon_{2,y}$ are scaling constants to be determined, and $\hat{r}, \hat{z}, \hat{t}, \hat{x}, \hat{y}_1$, and $\hat{y}_2$ are non-dimensional variables. Again we get the relations $X_L(r,z) = \varepsilon_x \hat{x}(\varepsilon_r \hat{r} + a, \varepsilon_z \hat{z}) = \varepsilon_x \hat{x}\left(\varepsilon_r^{-1}(r-a), \varepsilon_z^{-1} z\right)$,

$Y_{L,1}(r,z) = \varepsilon_{1,y}\hat{y}_1\left(\varepsilon_r^{-1}(r-a), \varepsilon_z^{-1}z\right)$, and $Y_{L,2}(r,z) = \varepsilon_{2,y}\hat{y}_2\left(\varepsilon_r^{-1}(r-a), \varepsilon_z^{-1}z\right)$. Again the gradient operator is also scaled as

$$\nabla X_L = \begin{pmatrix} 1/\varepsilon_r & 0 \\ 0 & 1/\varepsilon_z \end{pmatrix} \hat{\nabla}\varepsilon_x\hat{x}, \qquad \text{with} \qquad \hat{\nabla} = \begin{pmatrix} \frac{\partial}{\partial \hat{r}} & \frac{\partial}{\partial \hat{z}} \end{pmatrix}^\top.$$

For ease of presentation, we will separate the derivation into two parts. First, we will find the non-dimensionalised version of the differential equations. Here the choice of the scaling will not be explicit. This changes in the second part, where we present a scaled version of the boundary and initial conditions.

C.1 Scaled differential equations

The scaled equations can be found following the same steps as before. First consider the quantities

$$\left(\theta + \frac{b_X}{1+\kappa_{X,1}b_X Y_{L,1} + \kappa_{X,2}b_X Y_{L,2}}\right)\partial_t X_L = \frac{\varepsilon_x}{\varepsilon_t}\left(\theta + \frac{b_X}{1+\varepsilon_{1,y}\kappa_{X,1}b_X\hat{y}_1 + \varepsilon_{2,y}\kappa_{X,2}b_X\hat{y}_2}\right)\frac{\partial \hat{x}}{\partial \hat{t}} \tag{.1a}$$

$$\frac{\kappa_{X,1}b_X^2 X_L}{\left(1+\kappa_{X,1}b_X Y_{L,1} + \kappa_{X,2}b_X Y_{L,2}\right)^2}\partial_t Y_{L,1} = \frac{\varepsilon_x}{\varepsilon_t}\frac{\varepsilon_{1,y}\kappa_{X,1}b_X^2\hat{x}}{\left(1+\varepsilon_{1,y}\kappa_{X,1}b_X\hat{y}_1 + \varepsilon_{2,y}\kappa_{X,2}b_X\hat{y}_2\right)^2}\frac{\partial \hat{y}_1}{\partial \hat{t}} \tag{.1b}$$

$$\frac{\kappa_{X,2}b_X^2 X_L}{\left(1+\kappa_{X,1}b_X Y_{L,1} + \kappa_{X,2}b_X Y_{L,2}\right)^2}\partial_t Y_{L,2} = \frac{\varepsilon_x}{\varepsilon_t}\frac{\varepsilon_{2,y}\kappa_{X,2}b_X^2\hat{x}}{\left(1+\varepsilon_{1,y}\kappa_{X,1}b_X\hat{y}_1 + \varepsilon_{2,y}\kappa_{X,2}b_X\hat{y}_2\right)^2}\frac{\partial \hat{y}_2}{\partial \hat{t}} \tag{.1c}$$

Proceed to define the scaled constants $\hat{\kappa}_{X,1} = \varepsilon_{1,y}\kappa_{X,1}$, $\hat{\kappa}_{X,2} = \varepsilon_{2,y}\kappa_{X,2}$, and reuse the scaled vector $\hat{v}$ and the matrix $\hat{D}_x$, and then define the non-dimensionalised quantity $\hat{g}_X = {}^{\varepsilon_t}/_{\varepsilon_x} g_X$. This way we get from (.1) that

$$\begin{aligned}\left(\theta + \frac{b_X}{1+\hat{\kappa}_{X,1}b_X\hat{y}_1 + \hat{\kappa}_{X,2}b_X\hat{y}_2}\right)\frac{\partial \hat{x}}{\partial \hat{t}} &- \frac{\hat{\kappa}_{X,1}b_X^2\hat{x}}{\left(1+\hat{\kappa}_{X,1}b_X\hat{y}_1 + \hat{\kappa}_{X,2}b_X\hat{y}_2\right)^2}\frac{\partial \hat{y}_1}{\partial \hat{t}} \\ &- \frac{\hat{\kappa}_{X,2}b_X^2\hat{x}}{\left(1+\hat{\kappa}_{X,1}b_X\hat{y}_1 + \hat{\kappa}_{X,2}b_X\hat{y}_2\right)^2}\frac{\partial \hat{y}_2}{\partial \hat{t}} = \hat{\nabla}\cdot\left(\hat{D}_x\hat{\nabla}\hat{x} - \hat{x}\hat{v}\right) - \hat{g}_X.\end{aligned} \tag{.2}$$

Similarly, for (4.6b), we first get the relations

$$\left(\theta + \frac{b_{Y,1}}{1+\kappa_{Y,1}b_{Y,1}X_L}\right)\partial_t Y_{L,1} = \frac{\varepsilon_{1,y}}{\varepsilon_t}\left(\theta + \frac{b_{Y,1}}{1+\varepsilon_x\kappa_{Y,1}b_{Y,1}\hat{x}}\right)\frac{\partial \hat{y}_1}{\partial \hat{t}} \tag{.3a}$$

$$\frac{\kappa_{Y,1}b_{Y,1}^2 Y_{L,1}}{\left(1+\kappa_{Y,1}b_{Y,1}X_L\right)^2}\partial_t X_L = \frac{\varepsilon_{1,y}}{\varepsilon_t}\frac{\varepsilon_x\kappa_{Y,1}b_{Y,1}^2\hat{y}_1}{\left(1+\varepsilon_x\kappa_{Y,1}b_{Y,1}\hat{x}\right)^2}\frac{\partial \hat{x}}{\partial \hat{t}}. \tag{.3b}$$

Now define

$$\hat{\kappa}_{Y,1} = \varepsilon_x\kappa_{Y,1}, \qquad \hat{D}_{y,1} = \begin{pmatrix} \hat{D}_{Y,1,r} & 0 \\ 0 & \hat{D}_{Y,1,z} \end{pmatrix} = D_{Y,1}\varepsilon_t\begin{pmatrix} \varepsilon_r^{-2} & 0 \\ 0 & \varepsilon_z^{-2} \end{pmatrix}, \qquad \text{and} \qquad \hat{g}_{y,1} = \frac{\varepsilon_t}{\varepsilon_{1,y}}g_{Y,1}$$

to get from (.3) that

$$\left(\theta + \frac{b_{Y,1}}{1+\hat{\kappa}_{Y,1}b_{Y,1}\hat{x}}\right)\frac{\partial \hat{y}_1}{\partial \hat{t}} - \frac{\hat{\kappa}_{Y,1}b_{Y,1}^2\hat{y}_1}{\left(1+\hat{\kappa}_{Y,1}b_{Y,1}\hat{x}\right)^2}\frac{\partial \hat{x}}{\partial \hat{t}} = \hat{\nabla}\cdot(\hat{D}_{y,1}\hat{y}_1 - \hat{y}_1\hat{v}) - \hat{g}_{y,1}. \tag{.4}$$

Finally, for (4.6c) define

$$\hat{\kappa}_{Y,2} = \varepsilon_x\kappa_{Y,2}, \qquad \hat{D}_{y,2} = \begin{pmatrix}\hat{D}_{Y,2,r} & 0\\ 0 & \hat{D}_{Y,2,z}\end{pmatrix} = D_{Y,2}\varepsilon_t\begin{pmatrix}\varepsilon_r^{-2} & 0\\ 0 & \varepsilon_z^{-2}\end{pmatrix}, \qquad \text{and} \qquad \hat{g}_{y,2} = \frac{\varepsilon_t}{\varepsilon_{2,y}}g_{Y,2},$$

from which we get

$$\left(\theta + \frac{b_{Y,2}}{1+\hat{\kappa}_{Y,2}b_{Y,2}\hat{x}}\right)\frac{\partial \hat{y}_2}{\partial \hat{t}} - \frac{b_{Y,2}^2\hat{\kappa}_{Y,2}\hat{y}_2}{\left(1+\hat{\kappa}_{Y,2}b_{Y,2}\hat{x}\right)^2}\frac{\partial \hat{x}}{\partial \hat{t}} = \hat{\nabla}\cdot(\hat{D}_{y,2}\hat{\nabla}\hat{y}_2 - \hat{y}_2\hat{v}) - \hat{g}_{y,2}. \tag{.5}$$

C.2 Scaled boundary and initial conditions

The choice of the scaling parameters come from the boundary conditions.

Here we will present the choice and development for the secretion of two exudates. The treatment is similar for the secretion of one.

Again, the derivation is straightforward from the base model. First, we note that for X_L we get, for one side of the boundary, that

$$\hat{D}_{X,r}\frac{\partial \hat{x}}{\partial \hat{r}} - \hat{v}_r\hat{x} = \hat{\alpha}_1\hat{x} \qquad \text{at } \hat{r}=0, \quad \hat{z}\in[\hat{L}_1 - \delta\hat{L}_{x,1}, \hat{L}_1]; \tag{.6a}$$

where we require $\alpha_1 = {}^{\varepsilon_r}/_{\varepsilon_t}\hat{\alpha}_1$, $\hat{L}_1 = \varepsilon_z^{-1}L_1$, and $\delta\hat{L}_{x,1} = \varepsilon_z^{-1}\delta L_{X,1}$. Similarly, the other side of the boundary follows

$$\hat{D}_{X,r}\frac{\partial \hat{x}}{\partial \hat{r}} - \hat{v}_r\hat{x} = -\hat{\alpha}_2\hat{x} \qquad \text{at } \hat{r}=1, \quad \hat{z}\in[\hat{L}_2 - \delta\hat{L}_{x,2}, \hat{L}_2]; \tag{.6b}$$

where we have selected $\varepsilon_r = w$, and a proper selection of constants as in the previous line.

The relationships for $Y_{L,1}$ and $Y_{L,2}$ are similar:

$$\hat{D}_{Y,1,r}\frac{\partial \hat{y}_1}{\partial \hat{r}} - \hat{v}_r\hat{y}_1 = -\hat{F}_{1,1}(t) \qquad \text{at } \hat{r}=0, \quad \hat{z}\in[\hat{L}_1 - \delta\hat{L}_{y,1,1}, \hat{L}_1], \tag{.6c}$$

$$\hat{D}_{Y,2,r}\frac{\partial \hat{y}_2}{\partial \hat{r}} - \hat{v}_r\hat{y}_2 = -\hat{F}_{2,1}(t) \qquad \text{at } \hat{r}=0, \quad \hat{z}\in[\hat{L}_1 - \delta\hat{L}_{y,2,1}, \hat{L}_1], \tag{.6d}$$

$$\hat{D}_{Y,1,r}\frac{\partial \hat{y}_1}{\partial \hat{r}} - \hat{v}_r\hat{y}_1 = \hat{F}_{1,2}(t) \qquad \text{at } \hat{r}=1, \quad \hat{z}\in[\hat{L}_2 - \delta\hat{L}_{y,1,2}, \hat{L}_2], \tag{.6e}$$

$$\hat{D}_{Y,2,r}\frac{\partial \hat{y}_2}{\partial \hat{r}} - \hat{v}_r\hat{y}_2 = \hat{F}_{2,2}(t) \qquad \text{at } \hat{r}=1, \quad \hat{z}\in[\hat{L}_2 - \delta\hat{L}_{y,2,2}, \hat{L}_2]; \tag{.6f}$$

where appropriate quantities are selected. For instance $\hat{F}_{1,1} = \frac{\varepsilon_t}{\varepsilon_r\varepsilon_{1,y}}F_{Y,1,1}$.

For the other scaling parameters, notice that if we again pick $\varepsilon_z = L_{t_{\max}}$, again $\hat{z}$ will be in the range $[0,-1]$. This choice implies that $\max_t\{|\hat{L}_1|, |\hat{L}_2|\}$ should be 1, where we have

$$\hat{L}_1 = \hat{L}_1(\hat{t}) = \frac{1}{\varepsilon_z}(L_{1,0} + G_1\varepsilon_t\hat{t}) = \hat{L}_{1,0} + \hat{G}_1\hat{t}, \qquad \hat{L}_{1,0} = \varepsilon_z^{-1}L_{1,0}, \qquad \hat{G}_1 = \varepsilon_t\varepsilon_z^{-1}G_1, \tag{.7}$$

$$\hat{L}_2 = \hat{L}_2(\hat{t}) = \frac{1}{\varepsilon_z}(L_{2,0} + G_2\varepsilon_t\hat{t}) = \hat{L}_{2,0} + \hat{G}_2\hat{t}, \qquad \hat{L}_{2,0} = \varepsilon_z^{-1}L_{2,0}, \qquad \hat{G}_2 = \varepsilon_t\varepsilon_z^{-1}G_2; \tag{.8}$$

and we can further select $\varepsilon_t = t_{\max}$ to finally have $\hat{t}$ in the range $[0, 1]$. As a result, we have selected scaling parameters such that the system of partial differential equations is defined in $[0, 1] \times [0, -1] \times [0, 1]$. Lastly, the initial conditions are scaled as $(\hat{x}_0, \hat{y}_{1,0}, \hat{y}_{2,0}) = (\varepsilon_x^{-1}X_L^0, \varepsilon_{1,y}^{-1}Y_{L,1}^0, \varepsilon_{2,y}^{-1}Y_{L,2}^0)$.

Observe that again we can use parameters ε_x, $\varepsilon_{1,y}$, and $\varepsilon_{2,y}$ to calibrate the effects of $\hat{x}$ and $\hat{y}$ in all of the nonlinear terms in the above equations.